

Building a Maxey–Riley framework for surface ocean inertial particle dynamics

F. J. Beron-Vera,^{1, a)} M. J. Olascoaga,² and P. Miron¹

¹⁾*Department of Atmospheric Sciences, Rosenstiel School of Marine and Atmospheric Science, University of Miami, Miami, Florida 33149, USA*

²⁾*Department of Ocean Sciences, Rosenstiel School of Marine and Atmospheric Science, University of Miami, Miami, Florida 33149, USA*

(Dated: Started: March 2, 2019; this version: January 19, 2023.)

A Maxey–Riley set for surface ocean inertial (i.e., buoyant, finite-size) particle dynamics is derived by vertically integrating the original Maxey–Riley set, adapted to account for Earth’s rotation and sphericity effects, across a sufficiently small spherical particle, floating at an unperturbed air–sea interface with unsteady nonuniform winds and ocean currents above and below, respectively. The inertial particle velocity is shown to exponentially decay in time to a velocity that lies close to an average of seawater and air velocities, weighted by a function of the seawater-to-particle density ratio. Such a weighted average velocity turns out to fortuitously be of the type commonly discussed in the search-and-rescue literature, which alone cannot explain the observed role of anticyclonic mesoscale eddies as traps for marine debris or the formation of great garbage patches in the subtropical gyres, phenomena dominated by finite-size effects. A heuristic extension of the theory is proposed to describe the motion of nonspherical particles by means of a simple shape factor correction, and recommendations are made for incorporating wave-induced Stokes drift, consistently accounting for memory effects in the presence of recurrent motions, and allowing for inhomogeneities of the carrying fluid density. The new Maxey–Riley set outperforms an ocean adaptation that ignored wind drag effects and the first reported adaption that attempted to incorporate them.

PACS numbers: 02.50.Ga; 47.27.De; 92.10.Fj

CONTENTS		Acknowledgments	16
I. Introduction	1	A. Inertial ocean dynamics on the sphere	16
II. Setup	3	B. Attractivity and instability conditions for neutrally buoyant particles	17
III. The Maxey–Riley set	4	C. Slow manifold reduction in the standard fluid mechanics setting with lift force	18
A. The original fluid mechanics formulation	4	References	18
B. The proposed adaptation to surface ocean dynamics	5		
IV. Behavior at limiting particle buoyancies and small-size asymptotics	7		
A. The neutrally buoyant case	7	I. INTRODUCTION	
B. The maximally buoyant case	8		
C. Slow manifold reduction	8		
V. Reality check	10		
A. Mesoscale eddies as flotsam traps	10		
B. Great garbage patches	11		
VI. Discussion	13		
A. Shape corrections	13		
B. Stokes drift	14		
C. Memory effects	15		
D. Density inhomogeneities	15		
VII. Concluding remarks	16		

^{a)}Electronic mail: fberon@miami.edu

The study of the motion of *inertial* (i.e., buoyant, finite-size) particles was pioneered by Stokes¹ by solving the linearized Navier–Stokes equations for the oscillatory motion of a small solid sphere (pendulum) immersed in a fluid at rest. This was followed by the efforts of Basset², Boussinesq³, and Oseen⁴ to model a solid sphere settling under gravity, also in a quiescent fluid. Tchen⁵ extended these efforts to model motion in nonuniform unsteady flow by writing the resulting equation, known as the BBO equation, on a frame of reference moving with the fluid. Several corrections to the precise form of the forces exerted on the particle due to the solid–fluid interaction were made along the years⁶ until the now widely accepted form of the forces was derived by Maxey and Riley⁷ from first principles, following an approach introduced by Riley⁸, and independently and nearly simultaneously by Gatignol⁹. The resulting equation, with a

correction made by Auton, Hunt, and Prud'homme¹⁰, is commonly referred to as the *Maxey–Riley equation*.

The Maxey–Riley set is a classical mechanics second Newton's law that provides the de-jure framework for modeling inertial particle motion in fluid mechanics^{11–13} (and references therein). Conveniently given in the form of an ordinary differential equation, it has for instance facilitated the understanding of why buoyant particles can behave quite differently than fluid (i.e., neutrally buoyant, infinitesimally small) particles no matter how small^{14,15}. Such an understanding would have been very difficult to be attained by solving the numerically expensive Navier–Stokes partial differential equations with a moving boundary.

Understanding inertial particle motion is crucial in oceanography for a number of reasons. These include a need of improving the success of search-and-rescue operations at sea^{16,17}, better understanding the drift of macroalgae^{18,19}, or the motion of flotsam in general such as plastic litter^{20,21}, airplane wreckage^{22,23}, tsunami debris^{24,25}, and even sea-ice pieces in a warming climate²⁶.

With the well-founded expectation that the Maxey–Riley set can provide insight into inertial particle motion in the ocean, two ocean adaptations of the set were recently proposed (additional applications in oceanography have been reported^{27–30}, but we do not discuss them here as these mostly deal with settling of particles under gravity or biological problems rather than motion near the ocean surface). Beron-Vera *et al.*³¹ included Earth rotation effects, and restricting to quasigeostrophic carrying flow, investigated the motion of inertial particles near mesoscale eddies. These authors found that mesoscale eddies with coherent material boundaries^{32–34} can attract or repel inertial particles depending on the buoyancy of the particles and the polarity of the eddies. The result was formalized by Haller *et al.*³⁴ by providing rigorous conditions under which finite-time attractors or repellers can be found inside eddies. The prediction was supported in Beron-Vera *et al.*³¹ by an observation in the Pacific Ocean of two submerged drifting buoys (floats), which, deployed nearby inside a anticyclonic mesoscale eddy, one remained looping inside the eddy while the other was expelled away from it. According to the theory heavy (light) inertial particles should be attracted (repelled) by anticyclonic eddies and vice versa by cyclonic eddies. And indeed the observation adhered to the theoretical result since the float that remained trapped in the eddy was seen to take a slightly descending path while the float that escaped the eddy took a slightly ascending path. While some evidence was presented in Beron-Vera *et al.*³¹ for similar behavior at the ocean surface, the dynamics there can be expected to be different than those below due to the wind action. A consequence of this is the inability of the ocean adaptation of the Maxey–Riley set by Beron-Vera *et al.*³¹ to describe the accumulation of marine debris into large patches in the subtropical gyres²¹.

The above motivated Beron-Vera, Olascoaga, and Lumpkin³⁵ to extend the theory to account for the combined effect on a particle of ocean current and wind drag. With this in mind, Beron-Vera, Olascoaga, and Lumpkin³⁵ proceeded heuristically by modeling the particle piece immersed in the seawater (air) as a sphere of the fractional volume that is immersed in the seawater (air), and assuming that it evolves according to the Maxey–Riley set. The subspheres were advected together and the forces acting on each of them were calculated at the same position. This heuristics resulted in a Maxey–Riley set, which, including Earth's rotation and sphericity effects, predicted the formation of great garbage patches in the subtropical gyres as a phenomenon dominated by inertial effects, rather than Ekman convergence as commonly argued^{36,37}. The Maxey–Riley equation for surface ocean inertial particle dynamics by Beron-Vera, Olascoaga, and Lumpkin³⁵, just as that for subsurface ocean inertial particle dynamics by Beron-Vera *et al.*³¹, predicts accumulation of (light) particles into cyclonic eddies and repulsion from anticyclonic eddies. However, recent in-situ observations are showing the contrary³⁷, consistent with the traditional paradigm³⁸ that does not account for inertial effects, which represents a puzzle. On the other hand, the neutrally buoyant limit of the Maxey–Riley equation of Beron-Vera, Olascoaga, and Lumpkin³⁵ does not coincide with that of the standard Maxey–Riley set as it includes descriptors of the air component of the carrying flow when the particle is completely immersed in the seawater below the surface. Furthermore, results from a dedicated experiment involving satellite-tracked floating objects of different buoyancies, sizes, and shapes³⁹ are showing little trajectory prediction skill for the Maxey–Riley set proposed by Beron-Vera, Olascoaga, and Lumpkin³⁵.

To improve the description of inertial particle motion at the air–sea interface provided by the Maxey–Riley set, a new ocean adaptation of the set is proposed here. The new set is obtained by vertically integrating the original set, appropriately extended to represent Earth's rotation and sphericity effects, across a sufficiently small spherical particle which floats at an unperturbed air–sea interface with unsteady nonuniform winds and ocean currents above and below, respectively. The new set, while preserving the important capability of the one derived by Beron-Vera, Olascoaga, and Lumpkin³⁵ in predicting garbage patch formation, predicts concentration of particles inside anticyclonic eddies consistent with observations, thereby explaining this phenomenon as a result of inertial effects. As the Maxey–Riley set proposed by Beron-Vera, Olascoaga, and Lumpkin³⁵, the inertial particle velocity is shown to exponentially decay in time to a velocity that lies close to an average of seawater and air velocities, weighted by a certain function of the seawater-to-particle density ratio that conveys it additional margin for modeling in a wider range of conditions. This velocity coincidentally is of the type extensively discussed in the search-and-rescue literature and obtained mainly empiri-

cally or from considerations that are difficult to justify. In any case, the weighted average velocity alone cannot explain the observed role of anticyclonic mesoscale eddies as traps for marine debris or the formation of great garbage patches in the subtropical gyres, phenomena dominated by finite-size effects. A heuristic extension of the Maxey–Riley theory derived here to describe the motion of non-spherical particles is proposed, and recommendations are made for incorporating wave-induced Stokes drift, consistently accounting for memory effects in the presence of recurrent motions, and accounting for lateral gradients and time variations of the advecting fluid density.

The rest of the paper is organized as follows. Section 2 starts with the mathematical setup. In §3 we present the proposed ocean adaptation of the Maxey–Riley set after introducing and discussing the forcing terms involved. Limiting buoyancy behavior of the Maxey–Riley set and its small-size asymptotic dynamics (slow manifold reduction) are discussed in §4. The ability of the model derived to describe observed behavior is demonstrated in §5. Section 6 addresses corrections of the set to account for the motion of nonspherical particles, the incorporation of wave-induced drift, and the inclusion of memory effects and those produced by the carrying fluid density varying in space and time. Section 7 presents the conclusions of the paper. Finally, Appendix A includes the full spherical reduction, and Appendix B presents some mathematical details.

II. SETUP

Let $x = (x^1, x^2)$ with x_1 (resp., x_2) pointing eastward (resp., northward) be position on some domain D of the β plane, i.e., $D \subset \mathbb{R}^2$ rotates with angular speed $\frac{1}{2}f$ where $f = f_0 + \beta x^2$ is the Coriolis parameter; let z denote the vertical direction; and let t stand for time, ranging on some finite interval $I \subset \mathbb{R}$ (Figure 1). Consider a stack of two homogeneous fluid layers separated by an interface, assumed to be *fixed* at $z = 0$ Figure 1. The fluid in the bottom layer represents the seawater and has density ρ . The top-layer fluid is much lighter, representing the air; its density is $\rho_a \ll \rho$. Let μ and μ_a stand for dynamic viscosities of seawater and air, respectively. The seawater and air velocities vary in horizontal position and time, and are denoted $v(x, t)$ and $v_a(x, t)$, respectively. Consider finally a solid spherical particle, of radius a and density ρ_p , floating at the air–sea interface.

Let

$$\delta := \frac{\rho}{\rho_p}, \quad \delta_a := \frac{\rho_a}{\rho_p}. \quad (1)$$

Clearly, $\delta \gg \delta_a$. Let $\sigma \geq 0$ be the fraction of submerged (in seawater) particle volume. The emerged fraction then is $1 - \sigma$, which is sometimes referred to as *reserve buoyancy*. Static (in the *vertical*) stability of the particle

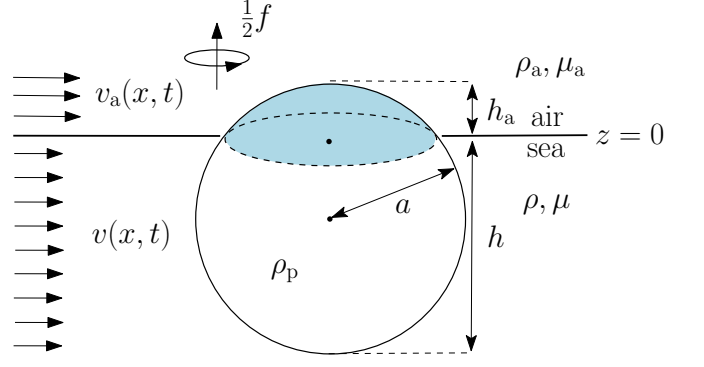


Figure 1. Solid spherical particle that floats at an assumed flat interface between homogeneous seawater and air, and is subjected to flow, added mass, and drag forces resulting from the action of unsteady, horizontally sheared ocean currents and winds. See text for variable and parameter definitions.

(Archimedes’ principle),

$$\sigma\delta + (1 - \delta)\delta_a = 1, \quad (2)$$

is satisfied for

$$\sigma = \frac{1 - \delta_a}{\delta - \delta_a}, \quad (3)$$

which requires

$$\delta \geq 1, \quad \delta_a \leq 1. \quad (4)$$

We will conveniently assume³⁵

$$\delta_a \ll 1, \quad (5)$$

so (3) can be well approximated by

$$\sigma = \delta^{-1}. \quad (6)$$

The height (h_a) of the emerged spherical cap can be expressed in terms of δ . This follows from equating its volume formula expressed in terms of a and h_a with the volume of the emerged spherical cap. To wit,

$$\frac{\pi h_a^2}{3}(3a - h_a) = (1 - \delta^{-1})\frac{4}{3}\pi a^3, \quad (7)$$

whose only physically meaningful root is

$$h_a/a = \Phi := \frac{i\sqrt{3}}{2} \left(\frac{1}{\varphi} - \varphi \right) - \frac{1}{2\varphi} - \frac{\varphi}{2} + 1 \quad (8)$$

where

$$\varphi := \sqrt[3]{i\sqrt{1 - (2\delta^{-1} - 1)^2} + 2\delta^{-1} - 1} \quad (9)$$

(Figure 2, top panel). The depth (h) of the submerged spherical cap,

$$h = (2 - \Phi)a. \quad (10)$$

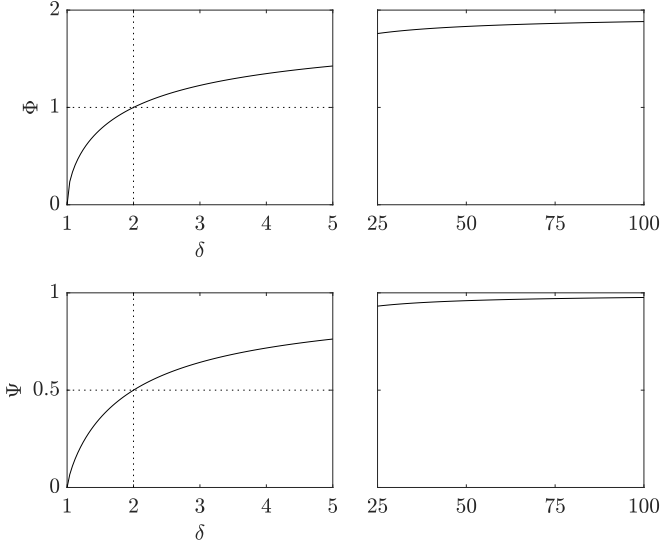


Figure 2. (top/bottom) Normalized by radius/area, height/projected area of emerged spherical particle cap as a function of the seawater-to-particle density ratio.

For a neutrally buoyant particle, i.e., $\delta = 1$, $\varphi = 0$ and thus $\Phi = 0$. Consequently, as expected, $h_a = 0$ (and hence $h = 2a$). Near neutrality, $\Phi = \frac{2\sqrt{3}}{3}\sqrt{\delta - 1} - \frac{2}{9}(\delta - 1) + O((\delta - 1)^2)$, which reveals the real nature of the root(s) of (7) explicitly⁴⁰. A half-emerged (equivalently, half-submerged) particle, namely, $h_a = a = h$, corresponds to $\delta = 2$. On the other hand, $h_a \rightarrow 2a$ (and thus $h \rightarrow 0$) slowly as $\delta \rightarrow \infty$.

For future reference, the projected (in the flow direction) area of the emerged spherical cap, A_a , can be readily seen to be given by

$$A_a = \pi\Psi a^2, \quad \Psi := \pi^{-1} \cos^{-1}(1 - \Phi) - \pi^{-1}(1 - \Phi) \times \sqrt{1 - (1 - \Phi)^2}, \quad (11)$$

a function of δ exclusively (Figure 2, bottom panel). In turn, the immersed projected area, denoted A , is equal to

$$A = \pi a^2 - A_a = \pi(1 - \Psi)a^2. \quad (12)$$

When $\delta = 1$, $A_a = 0$ (and hence $A = \pi a^2$), which immediately follows from $\Psi = \frac{16\sqrt{3}}{9\pi}(\delta - 1)^{3/4} + O((\delta - 1)^{5/4})$ as $\delta \rightarrow 1$. The situation in which $A_a = \frac{1}{2}\pi a^2$ corresponds to $\delta = 2$. Finally, $A_a \rightarrow \pi a^2$ (and thus $A \rightarrow 0$) slowly as $\delta \rightarrow \infty$.

We close the setup with a few remarks. Ignoring the vertical shear of the ocean currents (resp., winds) below (resp., above) the interface over the extent of the particle piece that is immersed in the seawater (resp., air) is a reasonable approximation under the assumption that the particle is small. On the other hand, that the interface remains flat at all times is clearly a strong assumption. Recommendations for incorporating the effects of wind-induced (Stokes) drift are given below. In turn, ignoring

lateral gradients and time variations of the carrying fluid density can be of consequence, particularly near frontal regions. Below we provide means for incorporating their effects as well.

III. THE MAXEY–RILEY SET

A. The original fluid mechanics formulation

The exact motion of *inertial particles* such as that in Figure 1 is controlled by the Navier–Stokes equation with moving boundaries as such particles are extended objects in the fluid with their own boundaries. This approach results in complicated partial differential equations which are extremely difficult—if not impossible—to solve and analyze.

Here we are concerned with the approximation, formulated in terms of an ordinary differential equation, provided by the Maxey–Riley equation, which, as noted in the Introduction, has become the de-jure fluid mechanics paradigm for inertial particle dynamics.

More specifically, the Maxey–Riley equation is a classical mechanics Newton’s second law with several forcing terms that describe the motion of solid spherical particles immersed in the unsteady nonuniform flow of a homogeneous viscous fluid. Normalized by particle mass, $m_p = \frac{4}{3}\pi a^3 \rho_p$, the relevant forcing terms for the *horizontal* motion of a sufficiently small particle are:

1. the *flow force* exerted on the particle by the undisturbed fluid,

$$F_{\text{flow}} = \frac{m_f}{m_p} \frac{Dv_f}{Dt}, \quad (13)$$

where $m_f = \frac{4}{3}\pi a^3 \rho_f$ is the mass of the displaced fluid (of density ρ_f), and $\frac{Dv_f}{Dt}$ is the material derivative of the fluid velocity (v_f) or its total derivative taken along the trajectory of a fluid particle, $x = X_f(t)$, i.e., $\frac{Dv_f}{Dt} = \left[\frac{d}{dt} v_f(x, t) \right]_{x=X_f(t)} = \partial_t v_f + (\nabla v_f) v_f$;

2. the *added mass force* resulting from part of the fluid moving with the particle,

$$F_{\text{mass}} = \frac{\frac{1}{2}m_f}{m_p} \left(\frac{Dv_f}{Dt} - \dot{v}_p \right), \quad (14)$$

where \dot{v}_p is the acceleration of an inertial particle with trajectory $x = X_p(t)$, i.e., $\dot{v}_p = \frac{d}{dt} [v_p(x, t)]_{x=X_p(t)} = \partial_t v_p$ where $v_p = \partial_t X_p = \dot{x}$ is the inertial particle velocity;

3. the *lift force*, which arises when the particle rotates as it moves in a (horizontally) sheared flow,

$$F_{\text{lift}} = \frac{\frac{1}{2}m_f}{m_p} \omega_f (v_f - v_p)^\perp, \quad (15)$$

where $\omega_f = \partial_1 v_f^2 - \partial_2 v_f^1$ is the (vertical) vorticity of the fluid and

$$w^\perp = Jw, \quad J := \begin{pmatrix} 0 & -1 \\ 1 & 0 \end{pmatrix} \quad (16)$$

for any vector w in \mathbb{R}^2 ; and

4. the *drag force* caused by the fluid viscosity,

$$F_{\text{drag}} = \frac{12\mu_f \frac{A_f}{\ell_f}}{m_p} (v_f - v_p), \quad (17)$$

where μ_f is the dynamic viscosity of the fluid, and $A_f (= \pi a^2)$ is the projected area of the particle and $\ell_f (= 2a)$ is the characteristic projected length, which we have intentionally left unspecified for future appropriate evaluation.

Except for the lift force (15), due to Auton⁴¹, the above forces are included in the original formulation by Maxey and Riley⁷⁹, yet with a form of the add mass term different than (14), which corresponds to the correction due to Auton, Hunt, and Prud'homme¹⁰. A Maxey–Riley model with lift force, which has not been so far considered in ocean dynamics despite its relevance in the presence of unbalanced (submesoscale) motions⁴², can be found in Montabone⁴³, Chapter 4 (cf. similar forms in Henderson, Gwynllwy, and Barengi⁴⁴, Sapsis *et al.*⁴⁵).

In writing (14) and (17), terms proportional to $\nabla^2 v_f$, so-called Faxen corrections, have been ignored. These account for the horizontal variation of the flow field across the particle, which is negligible for a particle with a radius much smaller than the typical length scale of the flow. Also, the complete set of Maxey–Riley forces involves an additional term, the Basset–Boussinesq history or memory term. This is an integral term that accounts for the lagging boundary layer developed around the particle. The memory term turns the Maxey–Riley set into a fractional differential equation that does not generate a dynamical system as the corresponding flow map does not satisfy a semi-group property^{46,47}. Numerical experimentation⁴⁸ reveals that the Basset history term mainly tends to slow down the inertial particle motion. More rigorously, Langlois, Farazmand, and Haller⁴⁷ show that the particle velocity decays algebraically, rather than exponentially as in the absence of the memory term, in time to a limit that is close, in the square of the particle's radius, to the carrying fluid velocity. The memory term cannot be neglected on sufficiently small particle assumption grounds^{47,49}, but it may be under the assumption that the time it takes a particle to return to a region that has visited earlier is long compared to the time scale of the flow⁵⁰, condition that should not be too difficult to be satisfied in the ocean, except, for instance, inside vortices.

B. The proposed adaptation to surface ocean dynamics

We first account for the geophysical nature of the fluid by including Coriolis force terms in (13) and (14)⁵¹. To wit,

$$F_{\text{flow}} \mapsto \frac{m_f}{m_p} \left(\frac{Dv_f}{Dt} + f v_f^\perp \right) \quad (18)$$

and

$$F_{\text{mass}} \mapsto \frac{\frac{1}{2}m_f}{m_p} \left(\frac{Dv_f}{Dt} + f v_f^\perp - \dot{v}_p - f v_p^\perp \right). \quad (19)$$

Geometric terms due to the planet's sphericity, which should be included when f is allowed to vary with x^2 , making (x^1, x^2) curvilinear rather than Cartesian⁵², were omitted as traditionally done for simplicity, yet recognizing that some consequences may be expected⁵³. Nevertheless, the full spherical form of the equations derived below, appropriate for operational use, is given in Appendix A.

Then, noting that fluid variables and parameters take different values when pertaining to seawater or air, e.g.,

$$v_f(x, z, t) = \begin{cases} v_a(x, t) & \text{if } z \in (0, h_a], \\ v(x, t) & \text{if } z \in [-h, 0), \end{cases} \quad (20)$$

we write

$$\dot{v}_p + f v_p^\perp = \langle F_{\text{flow}} \rangle + \langle F_{\text{mass}} \rangle + \langle F_{\text{lift}} \rangle + \langle F_{\text{drag}} \rangle, \quad (21)$$

where $\langle \cdot \rangle$ is an average over $z \in [-h, h_a]$.

Specifically,

$$\begin{aligned} \langle F_{\text{flow}} \rangle &= \frac{1}{2a} \int_{-h}^{h_a} \frac{m_f}{m_p} \left(\frac{Dv_f}{Dt} + f v_f^\perp \right) dz \\ &= \frac{1}{2a} \int_{(\Phi-2)a}^0 \frac{\delta^{-1} \frac{4}{3} \pi a^3 \rho}{\frac{4}{3} \pi a^3 \rho_p} \left(\frac{Dv}{Dt} + f v^\perp \right) dz \\ &\quad + \frac{1}{2a} \int_0^{\Phi a} \frac{(1 - \delta^{-1}) \frac{4}{3} \pi a^3 \rho_a}{\frac{4}{3} \pi a^3 \rho_p} \left(\frac{Dv_a}{Dt} + f v_a^\perp \right) dz \\ &= \frac{1}{2} (2 - \Phi) \left(\frac{Dv}{Dt} + f v^\perp \right) \\ &\quad + \frac{1}{2} (1 - \delta^{-1}) \Phi \delta_a \left(\frac{Dv_a}{Dt} + f v_a^\perp \right), \end{aligned} \quad (22)$$

where $\frac{D}{Dt}v$ (resp., $\frac{D}{Dt}v_a$) is understood to be taken along the trajectory of a seawater (resp., air) particle, obtained by solving $\dot{x} = v$ (resp., $\dot{x} = v_a$), namely, $\frac{D}{Dt}v = \partial_t v + (\nabla v)v$ (resp., $\frac{D}{Dt}v_a = \partial_t v_a + (\nabla v_a)v_a$). Taking into account that $\delta_a \ll 1$, (22) is well approximated by

$$\langle F_{\text{flow}} \rangle = \left(1 - \frac{\Phi}{2} \right) \left(\frac{Dv}{Dt} + f v^\perp \right). \quad (23)$$

Similarly,

$$\langle F_{\text{mass}} \rangle = \frac{1}{2a} \int_{-h}^{h_a} \frac{\frac{1}{2}m_f}{m_p} \left(\frac{Dv_f}{Dt} + f v_f^\perp - \dot{v}_p - f v_p^\perp \right) dz$$

$$\delta_a \ll 1 \quad \frac{1}{2} \left(1 - \frac{\Phi}{2} \right) \left(\frac{Dv}{Dt} + f v^\perp - \dot{v}_p - f v_p^\perp \right) \quad (24)$$

and

$$\langle F_{\text{lift}} \rangle = \frac{1}{2a} \int_{-h}^{h_a} \frac{\frac{1}{2}m_f}{m_p} \omega_f (v_f - v_p)^\perp dz$$

$$\delta_a \ll 1 \quad \frac{1}{2} \left(1 - \frac{\Phi}{2} \right) \omega (v - v_p)^\perp. \quad (25)$$

Now, to evaluate the drag force, appropriate projected length scales for the submerged and emerged particle pieces must be chosen. We conveniently take $\ell = kh$ and $\ell_a = k_a h_a$ for some $k, k_a > 0$. For instance, if $\delta = 1$ (resp., $\delta \rightarrow \infty$), namely, the particle is completely submerged below (resp., emerged above) the sea surface, $k = 1$ (resp., $k_a = 1$) is an appropriate choice so $\ell = 2a$ (resp., $\ell_a = 2a$). Thus, with this in mind,

$$\langle F_{\text{drag}} \rangle = \frac{1}{2a} \int_{-h}^{h_a} \frac{12\mu_f \frac{A_f}{\ell_f}}{m_p} (v_f - v_p) dz$$

$$= \frac{1}{2a} \int_{(\Phi-2)a}^0 \frac{12\mu \frac{\pi(1-\Psi)a^2}{k(2-\Phi)a}}{\frac{4}{3}\pi a^3 \rho_p} (v - v_p) dz$$

$$+ \frac{1}{2a} \int_0^{\Phi a} \frac{12\mu_a \frac{\pi\Psi a^2}{k_a\Phi a}}{\frac{4}{3}\pi a^3 \rho_p} (v_a - v_p) dz$$

$$= \frac{9\mu k^{-1}(1-\Psi)}{2\rho_p a^2} (v - v_p) + \frac{9\mu_a k_a^{-1}\Psi}{2\rho_p a^2} (v_a - v_p)$$

$$= \frac{3}{2} \left(1 - \frac{\Phi}{6} \right) \frac{u - v_p}{\tau}, \quad (26)$$

where

$$u := (1 - \alpha)v + \alpha v_a, \quad (27)$$

and the parameters

$$\tau := \frac{1 - \frac{1}{6}\Phi}{3(k^{-1}(1-\Psi) + \gamma k_a^{-1}\Psi)\delta} \cdot \frac{a^2}{\mu/\rho},$$

$$\alpha := \frac{\gamma k_a^{-1}\Psi}{k^{-1}(1-\Psi) + \gamma k_a^{-1}\Psi},$$

$$\gamma := \frac{\mu_a}{\mu}. \quad (28)$$

Finally, plugging (23)–(26) in (21), we obtain, after some algebraic manipulation,

$$\dot{v}_p + \left(f + \frac{1}{3}R\omega\right) v_p^\perp + \tau^{-1} v_p = R \frac{Dv}{Dt} + R \left(f + \frac{1}{3}\omega\right) v^\perp + \tau^{-1} u, \quad (29)$$

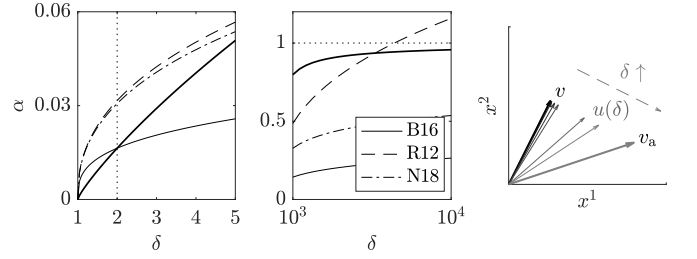


Figure 3. (left and middle) The behavior of the leeway factor α in (28) as a function of δ (with $\gamma = 1/60$ and $k = 1 = k_a$). B16, R12, and N18 indicate $\alpha(\delta)$ curves derived by Beron-Vera, Olascoaga, and Lumpkin³⁵, Röhrs *et al.*⁵⁴, and Nesterov⁵⁵, respectively. (right) The δ -weighted velocity in (27) for selected δ values.

where

$$R := \frac{1 - \frac{1}{2}\Phi}{1 - \frac{1}{6}\Phi}, \quad (30)$$

which is the explicit form of the Maxey–Riley set proposed in this paper. As a second-order ordinary differential equation in position, to integrate this classical mechanics motion law, not only initial position has to be specified but clearly also initial velocity.

In (28) parameter $\gamma > 0$ is less than unity ($\gamma \approx 1/60$, typically), while parameters α and τ behave as follows. First recall that $0 \leq \Phi < 2$, so $0 \leq \Psi < 1$ (cf. Figure 2). Then given that $k, k_a > 0$, it is easy to see that $0 \leq \alpha < 1$. More specifically, $\alpha = 0$ when $\delta = 1$ and $\alpha \rightarrow 1$ slowly as $\delta \rightarrow \infty$ (cf. thick curve(s) in the left and middle panels of Figure 3). Parameter τ , with units of time and representing a generalization of the so-called *Stokes time*⁵⁶, decays as a function of δ from $\frac{a^2}{3\mu/\rho}$ (since $k = 1$ is an appropriate choice when $\delta = 1$) to 0. Yet it can be brought arbitrarily close to 0 for finite δ if the inertial particle radius (a) is small enough. Finally, parameter R in (30) decays from 1 to 0 as δ increases from 1.

Because $\alpha \geq 0$, the linear span u in (27) can be interpreted as δ -weighted average of the seawater (v) and air (v_a) velocities. In fact, u coincides with v in the neutrally buoyant case ($\delta = 1$) in which the particle lies fully immersed in the seawater below the surface, whereas u approaches v_a as the particle lightens (i.e., as δ departs from unity) until it becomes fully exposed to the air above the sea surface (cf. Figure 2, right panel).

The original Maxey–Riley set was derived under the assumption that particle Reynolds number is less than unity, so the Stokes law for drag (17) can be used. The particle Reynolds number, $\text{Re}_p := \frac{V_{\text{slip}} \ell_f}{\mu_f / \rho_f}$ where V_{slip} is a measure of the magnitude of the *slip velocity*, i.e., that of the particle velocity (v_p) relative to that of the carrying flow (v_f). The asymptotic analysis of set (29) as $\tau \rightarrow 0$ (or, equivalently, $a \rightarrow 0$ if δ is kept finite) in the following section will reveal that an appropriate measure of V_{slip} is that of $|v_p - u|$. Furthermore, this asymptotic analysis will reveal that $v_p - u = O(\tau)$, so the use of the Stokes

drag law will be well justified for sufficiently small particles independent of the magnitude of the carrying flow velocity, effectively given by that of the δ -weighted velocity u , and the carrying fluid kinematic viscosity, taken as that of either the seawater or the air, or some average thereof.

As it follows from the aforementioned asymptotic analysis, in the sizeless particle case ($\tau = 0$), v_p coincides with u . The search-and-rescue literature⁵⁷ (and references therein) often models windage effects on the drift of objects as an additive contribution to the ocean current. In our notation this is $v_p = u$ for some α , commonly referred to as a *leeway factor*. Deduced empirically, α is taken as some fixed value in the range 1–5%^{22,58,59}. However, formulas depending on the projected areas of emerged and submerged pieces of the objects and their floatation characteristics have been proposed^{54,55}. These formulas, seemingly valid for arbitrary shaped objects, are obtained by assuming that the drag in the seawater is exactly balanced by that in the air above, a hard to justify assumption apparently first made by Geyer⁶⁰. Furthermore, these formulas consider a quadratic (in the slip particle) drag law. Such a law assumes that the particle is in Newton's (rather than Stokes') regime, which is valid for high object's Reynolds numbers⁶¹. Assuming that the (constant) drag coefficient is the same below and above the sea surface as in Nesterov⁵⁵, we show in the left and right panels of Figure 2 the resulting leeway factors as a function of δ for the case of spherical objects. Note for instance that the formula derived by Röhrs *et al.*^{54,62} exceeds unity in the $\delta \rightarrow \infty$ limit, while that of Nesterov⁵⁵ has not converged to unity for δ values for which a particle is almost completely exposed to the air (indeed, for $\delta = 10^3$, $\Phi = h_a/2a = 0.9816$). For smaller δ values the leeway factors derived by these authors exceed α in (28) for $k = 1 = k_a$. Figure 2 also shows the α curve obtained by Beron-Vera *et al.*³¹. Note that it lies below that one derived here, and it also very slowly tends to unity as $\delta \rightarrow \infty$. Because of this and the additional freedom in choosing k and k_a , the new formula for u has more margin (leeway!) than its predecessor for modeling in an wider range of conditions.

IV. BEHAVIOR AT LIMITING PARTICLE BUOYANCIES AND SMALL-SIZE ASYMPTOTICS

A. The neutrally buoyant case

Setting $\delta = 1$, the Maxey–Riley set (29) reduces to

$$\dot{v}_p + (f + \tfrac{1}{3}\omega) v_p^\perp + \tau^{-1} v_p = \frac{Dv}{Dt} + (f + \tfrac{1}{3}\omega) v^\perp + \tau^{-1} v, \quad (31)$$

with

$$\tau = \frac{a^2}{3\mu/\rho}. \quad (32)$$

The resulting set coincides *exactly* with the Maxey–Riley equation for neutrally buoyant particles as considered in Montabone⁴³, Chapter 7, which is the standard Maxey–Riley with Coriolis and lift forces included, but with Faxen corrections and memory term neglected¹³ (Section 4.1). This represents one additional improvement over the Maxey–Riley set for inertial surface ocean dynamics derived by Beron-Vera, Olascoaga, and Lumpkin³⁵, which did not account for lift force effects. That set evaluated at $\delta = 1$ has the same form as (31) if the lift force is excluded, yet with τ (in the notation of this paper) as in (32) times γ , which, being the air-to-seawater dynamic viscosity ratio, represents a strange element for the dynamics of particles that are completely submerged under the sea surface.

Such dynamics are quite special: they coincide, irrespective of the size of the particle (equivalently, the value of τ), with those of Lagrangian (seawater in the present case) particles if $v_p = v$ initially. To see this, following Babiano *et al.*¹⁴ closely, we add and subtract $(\nabla v)v_p$ to and from the right-hand-side of (31) so it recasts as the linear system

$$\dot{y} = Ay, \quad y := v_p - v, \quad A := -(\nabla v + (f + \tfrac{1}{3}\omega) J + \tau^{-1} \text{Id}), \quad (33)$$

where $\dot{v} = \frac{d}{dt}v = \partial_t v + (\nabla v)v_p$ is the total derivative of v taken along a particle trajectory, satisfying $\dot{x} = v_p$. Clearly, the trivial solution $y = 0$ is invariant under the dynamics. In other words,

$$\mathcal{N} := \{(x, t, v_p) \mid v_p = v(x, t), (x, t) \in D \times I\} \quad (34)$$

represents an invariant manifold (modulo its boundary, which has corners due to finiteness of I) that is unique as is set by the carrying flow, irrespective of the choice of τ .

However, in the nonrotating case ($f = 0$) and ignoring the lift force, the motion of neutrally buoyant particles of finite size is known from numerical analysis^{14,15} as well as laboratory experimentation⁴⁵ to possibly deviate from that of Lagrangian particles. Sapsis and Haller⁶³ rigorously addressed this problem by deriving a sufficient condition for global attractivity of \mathcal{N} in that case as well as a necessary condition for local instability of \mathcal{N} . It turns out that, because $J = -J^\top$, the same conditions as those obtained by Sapsis and Haller⁶³ are found in the present geophysical setting with Coriolis and lift forces (cf. Appendix B for details). In other words, these terms contribute to neither setting the attractivity property of \mathcal{N} , nor controlling the growth of perturbations off \mathcal{N} .

Specifically, let $S := \frac{1}{2}(\nabla v + (\nabla v)^\top)$ be the rate-of-strain tensor. Then for \mathcal{N} to be globally attracting, i.e., for v_p to approach v and hence neutrally buoyant finite-size particle motion to synchronize with seawater particle motion in the long run in D , $S + \tau^{-1} \text{Id}$ must be positive definite for all $x \in D$ over the time interval I , or, equivalently,

$$\tau < \frac{2}{\sqrt{S_n^2 + S_s^2 - \nabla \cdot v}}, \quad (35)$$

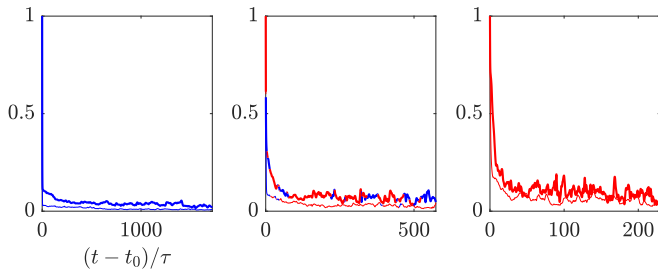


Figure 4. Normalized by initial value, ensemble-mean magnitude of the difference between neutrally particle velocity obeying (31) and seawater particle velocity, with the seawater velocity inferred from satellite-altimetry data, in the Gulf of Mexico over 15 Jan 2015 through 12 Apr 2016, and for Stokes time (τ) increasing from left to right. Thin curves correspond to solutions of (31) ignoring Coriolis and lift forces. Indicated in red (resp., blue) are periods during which the global attractivity condition (35) is satisfied (resp., violated).

where $S_n := \partial_1 v^1 - \partial_2 v^2$ and $S_s := \partial_2 v^1 + \partial_1 v^2$ respectively are normal and shear strain components, for all $x \in D$ over the time interval I . Clearly, for the latter to be realized over the finite-time interval I , v_p must initially lie sufficiently close to v , a restriction that is not required when $I = \mathbb{R}$ as in Sapsis and Haller⁶³. In the geophysically relevant incompressible case, (35) reduces to $\tau^2 > -\det S$ for all $(x, t) \in D \times I$. On the other hand, instantaneous divergence away from \mathcal{N} will take place where $S + \tau^{-1} \text{Id}$ is sign indefinite, or, equivalently, where (35) is violated.

We finalize this analysis with a test of the validity of the results. Rather than using kinematic representations of the carrying velocity v as done earlier⁶³, we here subject the results to a more demanding test by considering v as inferred using satellite altimetry measurements, in the Gulf of Mexico over 15 Jan 2015 through 12 Apr 2016. In this representation, the total sea surface height field, $\eta(x, t)$, is taken as the sum of a mean dynamic topography⁶⁴ and a sea-surface height anomaly field constructed from along-track satellite altimetry measurements⁶⁵. Assuming a geostrophic balance, $v = gf^{-1} \nabla^\perp \eta$.⁶⁶ The results of the test are presented in Figure 4, which shows, as a function of time, the magnitude of the difference between solution v_p of (31) and v , in an ensemble-mean sense. More specifically, using a time-step-adapting Runge-Kutta method with cubic interpolation, (31) was integrated from $t_0 = 15 \text{ Jan 2015}$ out to 12 Apr 2016 , starting from 10^3 initial locations x_0 distributed over the Gulf of Mexico domain, with $v_p(x_0, t_0)$ taken 25% larger than $v(x_0, t_0)$. Then v was interpolated along the trajectories of v_p , and an average $|v_p - v|$ along all trajectories was finally computed. This was done for three choices of Stokes time τ , increasing from the left to the right panel in Figure 4. Portions of the curves colored blue (resp., red) correspond to periods during which the global attractivity condition (35) is satisfied (resp., violated). Note that, as expected, the

convergence to v is increasingly hampered as local instability is more frequently realized during the evolution. Note too that a similar picture is obtained when Coriolis and lift forces are ignored (thin curves). The only visible difference in this case is that convergence is faster.

B. The maximally buoyant case

The limit $\delta \rightarrow \infty$ is dynamically less sophisticated than the $\delta = 1$ case of the previous section. In this limit, $\tau = 0$ and hence the Maxey-Riley set (29) reduces to simply

$$v_p = v_a. \quad (36)$$

A maximally buoyant particle lies on the assumed flat surface ocean and, irrespective of its size, its motion is synchronized at all times with that of air particle (i.e., Lagrangian) motion. In this limit, (29) and the Maxey-Riley set derived by Beron-Vera, Olascoaga, and Lumpkin³⁵ behave identically.

C. Slow manifold reduction

Because of the small particle size assumption, it is natural to investigate the asymptotic behavior of the Maxey-Riley set (29) as $\tau \rightarrow 0$, as it has been done for the Maxey-Riley set in its standard fluid mechanics form⁶⁷ and its earlier adaptations for ocean dynamics^{31,35,68}.

To carry the above investigation formally, we first rescale space and time by a characteristic length scale L and characteristic time scale $T = L/V$ where V is a characteristic velocity, and write the Maxey-Riley set (29) as a first-order differential equation, namely,

$$\dot{x} = v_p, \quad (37)$$

$$\tau \dot{v}_p = u - v_p - \tau \left(f + \frac{1}{3} R \omega \right) v_p^\perp + \tau R \frac{Dv}{Dt} + \tau R \left(f + \frac{1}{3} \omega \right) v^\perp. \quad (38)$$

All variables are here understood with no fear of confusion to be dimensionless. In particular, the dimensionless τ parameter,

$$\tau = \frac{(1 - \frac{1}{6} \Phi)}{3 \left(k^{-1} (1 - \Psi) + \gamma k_a^{-1} \Psi \right) \delta} \cdot \text{St}, \quad (39)$$

where $\text{St} := \frac{2}{9} \left(\frac{a}{L} \right)^2 \text{Re}$ is the Stokes number with $\text{Re} := \frac{VL}{\mu/\rho}$ the Reynolds number. We assume

$$\tau \ll 1. \quad (40)$$

Before proceeding, we note that the set (37)–(38) represents a nonautonomous four-dimensional dynamical system. As noted previously in this paper, to solve it one must initially specify both particle position and velocity, which is not known in general. Also, long backward-in-time integration, required in inverse modeling^{23,69}, is not

feasible because v_p/τ produces exponential growth with exponent τ^{-1} for decreasing t . This is known to cause numerical instability in the standard Maxey–Riley set⁶⁷.

Now, from (37)–(38) it is clear that v_p is a fast variable changing at $O(\tau^{-1})$ speed while x , changing at $O(\tau)$ speed, is a slow variable. As a consequence, (37)–(38) represents a singular perturbation problem. To regularize it, we introduce a fast timescale \mathbf{t} such that

$$\mathbf{t} := \frac{t - t_0}{\tau}, \quad (41)$$

where $t_0 \neq 0$ further enables nonautonomous singular perturbation analysis⁶⁷. Using a prime to denote differentiation with respect to \mathbf{t} , system (37)–(38) rewrites as an autonomous system in the extended phase space $D \times I \times \mathbb{R}^2$ with variables (x, φ, v_p) , where $\varphi := t_0 + \tau \mathbf{t}$, namely,

$$x' = \tau v_p, \quad (42)$$

$$\varphi' = \tau, \quad (43)$$

$$v_p' = u - v_p - \tau \left(f + \frac{1}{3} R \omega \right) v_p^\perp + \tau R \frac{Dv}{Dt} + \tau R \left(f + \frac{1}{3} \omega \right) v^\perp. \quad (44)$$

Setting $\tau = 0$ in (42)–(44), one finds that $x = x_0 = \text{const}$ and $\varphi = \varphi_0 = \text{const}$, and that $v_p = u(x, \varphi)$ forms a family of equilibria. This family fills a unique invariant attracting normally hyperbolic manifold (modulo its boundary),

$$\mathcal{S}_0 = \{(x, \varphi, v_p) \mid v_p = u(x, \varphi), x \in D, \varphi \in I\}. \quad (45)$$

Indeed, \mathcal{S}_0 is solely determined by u . Furthermore, integrating $v_p' = u(x_0, \varphi_0) - v_p$ from $t = t_0$ to $t > t_0$, it follows that $v_p(t) = u(x_0, t_0) + (v_p - u(x_0, t_0)) \cdot e^{\frac{t_0 - t}{\tau}}$, which shows that \mathcal{S}_0 is invariant under the dynamics of the $\tau = 0$ limit of (42)–(44) and also attracts all its solutions exponentially fast.

Assume that v and v_a , and hence their δ -weighted average u , are C^r smooth (i.e., r times continuously differentiable) in their arguments with $r > 1$. Autonomous geometric singular perturbation analysis results by Fenichel⁷⁰, extended by Haller and Sapsis⁶⁷ to the nonautonomous case, guarantee the existence of a manifold, \mathcal{S}_τ , for the $\tau \neq 0$ form of set (42)–(44) that lies $O(\tau)C^r$ -close to \mathcal{S}_0 , which having a Taylor expansion form, viz.,

$$\begin{aligned} \mathcal{S}_\tau := \{(x, \varphi, v_p) \mid v_p = u(x, \varphi) + \sum_1^r \tau^n u_n(x, \varphi) \\ + O(\tau^{r+1}), (x, \varphi) \in D \times I\}, \end{aligned} \quad (46)$$

is unique (up an error that is transcendentally small for sufficiently long $t - t_0$), invariant (with trajectories only possibly leaving \mathcal{S}_τ through its boundary), and furthermore exponentially attracts all solution of (42)–(44). The manifold \mathcal{S}_τ is referred to as *slow manifold*⁷¹ because

(42)–(44) restricted to \mathcal{S}_τ is as slowly varying system of the form

$$x' = \tau v_p|_{\mathcal{S}_\tau} = \tau u(x, \varphi) + \sum_1^r \tau^{n+1} u_n(x, \varphi) + O(\tau^{r+2}). \quad (47)$$

The functions $u_n(x, \varphi)$ are found as follows. First, one differentiates with respect to \mathbf{t} equation (C.7) defining the slow manifold \mathcal{S}_τ , to wit,

$$\begin{aligned} v_p' &= [(\nabla u)x' + \partial_\varphi u \varphi' + \sum_1^r \tau^n ((\nabla u_n)x' + \partial_\varphi u_n \varphi') \\ &\quad + O(\tau^{r+1})]_{\mathcal{S}_\tau} \\ &= \tau \frac{Du}{Dt} + \sum_{n=2}^r \tau^n \left(\partial_t u_{n-1} + (\nabla u_{n-1})u + (\nabla u)u_{n-1} \right. \\ &\quad \left. + \sum_{m=1}^{n-2} (\nabla u_m)u_{n-m-1} \right) + O(\tau^{r+2}), \end{aligned} \quad (48)$$

where $\frac{Du}{Dt}$ is understood to be taken along a trajectory of u , obtained by solving $\dot{x} = u$, i.e., $\frac{Du}{Dt} u = \partial_t u + (\nabla u)u$. Then restricting (44) to \mathcal{S}_τ , i.e.,

$$\begin{aligned} v_p' &= \left[u - v_p - \tau \left(f + \frac{1}{3} R \omega \right) v_p^\perp + \tau R \frac{Dv}{Dt} + \tau R \left(f + \frac{1}{3} \omega \right) v^\perp \right]_{\mathcal{S}_\tau} \\ &= - \sum_1^r \tau^n u_n - \tau \left(f + \frac{1}{3} R \omega \right) \left(u^\perp + \sum_1^r \tau^n u_n^\perp \right) + \tau R \frac{Dv}{Dt} \\ &\quad + \tau R \left(f + \frac{1}{3} \omega \right) v^\perp + O(\tau^{r+2}), \end{aligned} \quad (49)$$

and equating equal τ -power terms in (48) and (49), we obtain

$$u_1 = R \frac{Dv}{Dt} + R \left(f + \frac{1}{3} \omega \right) v^\perp - \frac{Du}{Dt} - \left(f + \frac{1}{3} R \omega \right) u^\perp \quad (50)$$

$$\begin{aligned} u_n &= - \left(f + \frac{1}{3} R \omega \right) u_{n-1}^\perp \\ &\quad - \partial_t u_{n-1} - (\nabla u_{n-1})u - (\nabla u)u_{n-1} \\ &\quad - \sum_{m=1}^{n-2} (\nabla u_m)u_{n-m-1}, \quad n \geq 2. \end{aligned} \quad (51)$$

So the Maxey–Riley set (29) on the slow manifold \mathcal{S}_τ reads

$$\dot{x} = v_p = u(x, t) + \sum_1^r \tau^n u_n(x, t) + O(\tau^{r+1}) \quad (52)$$

with $u_n(x, t)$ as given in (50)–(51). Switching back to dimensional variables, the leading-order contribution to above equation is given by

$$\dot{x} = v_p \sim u + \tau \left(R \frac{Dv}{Dt} + R \left(f + \frac{1}{3} \omega \right) v^\perp - \frac{Du}{Dt} - \left(f + \frac{1}{3} R \omega \right) u^\perp \right) \quad (53)$$

as $\tau \rightarrow 0$.

Several remarks are in order. Firstly, when $\delta = 1$, $\mathcal{S}_\tau = \{(x, t, v_p) \mid v_p = u(x, t), (x, t) \in D \times I\} \equiv \mathcal{N}$. This invariant manifold survives for any τ , but as we have seen above its stability may be lost for sufficiently large τ .

Second, rapid changes in time of the carrying flow velocity, represented by the δ -weighted velocity u , can lead to rapid changes on \mathcal{S}_τ , thereby hindering its efficacy in absorbing trajectories of the Maxey–Riley equation

over a finite time⁶⁷. Exceptions exist in rapidly changing carrying flows such as is the case of the vicinity of coherent Lagrangian vortices, which, depending on their polarity, admit finite-time attractors for inertial particles governed by the standard Maxey–Riley set with Coriolis force and a quasigeostrophic carrying flow^{31,34}. Inertial particles at the air–seawater interface governed by (53), as we demonstrate below, exhibit similar behavior but representing reality more tightly.

Third, unlike (29), its slow manifold reduction (53) is not subjected to numerical blowup during long backward-time integration. Furthermore, according to Theorem 2 of Sapsis and Haller⁶³, the starting position $x(t_0)$ of any solution $(x(t), v_p(t))$ may be recovered with $O(\tau)$ precision.

Fourth, constituting a two-dimensional nonautonomous dynamical system, the reduced Maxey–Riley (53) is advantageous for other reasons as well. Its integration is numerically less expensive than that of the full four-dimensional Maxey–Riley (53) set. It requires specification of initial positions of the particles exclusively. And furthermore, representing a simpler model, it can provide insight on sufficiently small particle motion that is difficult—if not impossible—to be gained from the analysis of the full model equations, as we show below.

Lastly, we note one difference with the slow manifold of the Maxey–Riley set in its standard fluid mechanics setting with lift force. As we show in Appendix C, the lift force makes an $O(\tau^2)$ contribution to the slow manifold in that setting. This is unlike the slow manifold in the present setting, in which case the contribution is $O(\tau)$.

We close this section by presenting a test of the validity of the slow manifold reduction developed above. As above, rather than relying on kinematic models of v and v_a , we carry out this test using altimetry-derived v , in the Gulf of Mexico over 15 Jan 2015 through 12 Apr 2016, and v_a as given by a blend of multiple-satellite observations over the same period⁷². Figure 5 shows, as a function of time, the ensemble-mean magnitude of $|v_p - v_p|_{S_\tau}|$. More specifically, we numerically integrated (using a time-set-adapting Runge–Kutta method with cubic interpolation) the full Maxey–Riley set (29) from $t_0 = 15$ Jan 2015 out to 12 Apr 2016 starting on 10^3 locations x_0 distributed over the Gulf of Mexico with $v_p(x_0, t_0) = 0$. Then v_p in (53) was interpolated along the resulting trajectories, and the average of $|v_p - v_p|_{S_\tau}|$ along all trajectories was computed. While the convergence to the slow manifold can be faster or slower for individual trajectories for the reasons noted above, in an ensemble-mean sense near-monotonic convergence is quite well realized over a roughly three-month period. This provides good support to the slow manifold reduction.

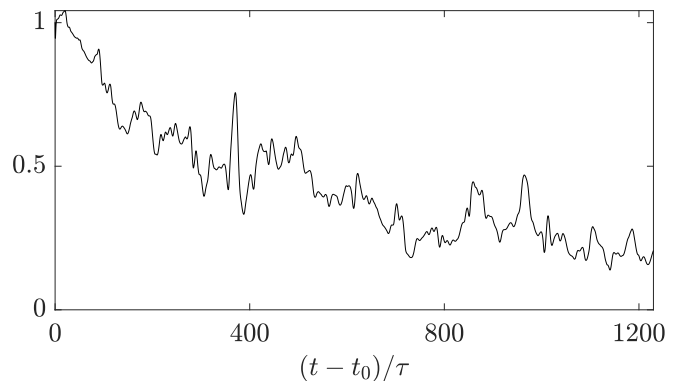


Figure 5. Normalized by initial value, ensemble-mean magnitude of the difference between the inertial particle velocity obeying the Maxey–Riley set (29) and the particle velocity restricted to its slow manifold (53), assuming ocean currents inferred from satellite-altimetry data and winds estimated from a blend of multiple-satellite observations, in the Gulf of Mexico over 15 Jan 2015 through 12 Apr 2016.

V. REALITY CHECK

A. Mesoscale eddies as flotsam traps

Using in-situ measurements from sea campaign Expedition 7th Continent in the North Atlantic subtropical gyre, data from satellite observations and models, Brach *et al.*³⁷ recently provided evidence that mesoscale anticyclonic eddies are more efficient at trapping flotsam within than cyclonic ones. Indeed, they found microplastic concentrations nearly ten times higher in an anticyclonic eddy surveyed than in a nearby cyclonic eddy. This phenomenon is predicted by the Maxey–Riley set proposed here.

Specifically, suppose that there are no winds ($v_a = 0$) and the ocean flow is quasigeostrophic. To wit, $v = \nabla^\perp \psi + O(\text{Ro}^2)$, $\partial_t v = O(\text{Ro}^2)$, and $f = f_0 + O(\text{Ro})$, where ψ is a streamfunction (e.g., $\psi = g f_0^{-1} \eta$) and $\text{Ro} = V/L|f_0| > 0$ small is the Rossby number⁵². Under these conditions, to the lowest order in Ro , the reduced Maxey–Riley set (53) simplifies to

$$\dot{x} = v_p \sim (1 - \alpha) \nabla^\perp \psi + \tau f_0 R \nabla \psi. \quad (54)$$

As defined by Haller *et al.*³⁴, a *rotationally coherent vortex* is a material region $U(t)$, $t \in [t_0, t_0 + T] \subset I$, enclosed by the outermost, sufficiently convex isoline of the Lagrangian averaged vorticity deviation (LAVD) field enclosing a local maximum. For the quasigeostrophic flow above, the LAVD is given by

$$\text{LAVD}_{t_0}^t(x_0) := \int_{t_0}^t |\nabla^2 \psi(F_{t_0}^s(x_0), s) - \overline{\nabla^2 \psi}(s)| \, ds, \quad (55)$$

where $F_{t_0}^t(x_0)$ is a trajectory of $\nabla^\perp \psi$ starting from x_0 at t_0 and the overline represents an average on D . As a consequence, the elements of the boundaries of such material

regions $U(t)$ complete the same total material rotation relative to the mean material rotation of the whole fluid mass in the domain D that contains them. This property of the boundaries is observed³⁴ to restrict their filamentation to be mainly tangential under advection from t_0 to $t_0 + T$.

Assume that D is large enough so $\overline{\nabla^2 \psi}$ nearly vanishes and bear in mind that $R > 0$. Then applying on (54) Theorem of 2 of Haller *et al.*³⁴, which essentially is an application of Liouville's theorem, one finds that a trajectory launched from a nondegenerate maximum x_0^* of $\text{LAVD}_{t_0}^{t_0+T}(x_0)$ attracts or repel trajectories of (54) depending on the sign of

$$f_0 \nabla^2 \psi(F_{t_0}^t(x_0^*), t, t) \quad (56)$$

over the time interval $[t_0, t_0 + T]$. More precisely, a rotationally coherent quasigeostrophic vortex $U(t)$ will contain an attractor (resp., repeller) over $[t_0, t_0 + T]$ staying $O(\tau)$ -close to its center $F_{t_0}^t(x_0^*)$ if (56) is negative (resp., positive). In other words, cyclonic (resp., anticyclonic) mesoscale such eddies disperse away (resp., concentrate within) inertial particles floating at the surface of the ocean. This result, which holds in the presence of a sufficiently calm uniform wind, is consistent with the observations reported by Brach *et al.*³⁷.

The earlier oceanic implementations^{31,35} of the Maxey–Riley formalism predict the behavior that is at odds with the above result. This may be a consequence of the heuristics considered by Beron-Vera, Olascoaga, and Lumpkin³⁵ being too restrictive. The case of Beron-Vera *et al.*³¹ is different because the only adaptation made was the inclusion of the Coriolis force. As considered, then, the set is not in principle meant to be valid for a particle floating at the sea surface, but rather for a particle immersed in a fluid as in the standard formulation. Indeed, that set does not seem possible to be obtained as a limit of the set derived here except for neutrally buoyant particles.

We finally note that Beron-Vera *et al.*³¹ present observational evidence of *Sargassum* (a pelagic brown algae) accumulating in a cold-core (i.e., cyclonic) Gulf Stream ring (eddy), which seems at odds with the observations discussed by Brach *et al.*^{37,19}. An important difference with microplastic particles is that *Sargassum* presents in the form of mats, which are better modeled as *networks* of buoyant particles than as individual particles. Work in progress⁷³ is revealing that *elastic chains* of sufficiently small buoyant particles evolving under the Maxey–Riley set derived here collect in cyclonic rotationally coherent quasigeostrophic eddies provided that the chains are stiff enough.

B. Great garbage patches

The NOAA's Global Drifter Program (GDP) is an array of drifting buoys used to measure the near surface ocean Lagrangian circulation⁷⁴. A GDP drifter follows

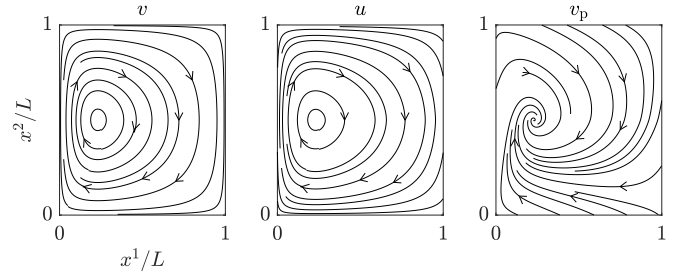


Figure 6. Streamlines of the Stommel wind-driven circulation model velocity (left), the δ -weighted velocity resulting from this velocity and the wind field that drives the Stommel gyre (middle), and dominant part of inertial particle velocity on the slow manifold of the Maxey–Riley set resulting from feeding the later with the aforementioned seawater and air velocities (right).

the Surface Velocity Program design⁷⁵, with a spherical float, which includes a transmitter to relay data via satellite, tethered to a holey sock drogue (sea anchor), centered at 15 m depth. Beron-Vera, Olascoaga, and Lumpkin³⁵ noted that GDP drifters have lost their drogues exhibit different time-asymptotic behavior than those that have not along their lifetime. More specifically, the undrogued drifters tend in the long run to accumulate in the centers of the subtropical gyres, most notably the Atlantic and Pacific subtropical gyres. By contrast drogued drifters tend to acquire more heterogeneous distributions in the long term. The regions where undrogued drifters concentrate coincide with the regions where microplastics maximize their densities as observations reveal²¹. In particular, the region where flotsam accumulates in the North Pacific is referred to as the Great Pacific Garbage Patch⁷⁶. We proceed to show that the Maxey–Riley set proposed here is able to predict “garbage patches” consistent with observed behavior, thereby allowing to interpret this behavior as produced by inertial effects as suggested by Beron-Vera, Olascoaga, and Lumpkin³⁵ using an early version of the set derived here.

We first do this by considering as in Beron-Vera, Olascoaga, and Lumpkin³⁵ the conceptual model of wind-driven circulation due to Stommel⁷⁷. The steady flow in such a barotropic model is quasigeostrophic, i.e., $v = \nabla^\perp \psi(x) = O(\text{Ro})$, and has an anticyclonic basin-wide gyre in the northern hemisphere, so $\omega = \nabla^2 \psi \leq 0$, driven by steady westerlies and trade winds, namely, $v_a = W(x^2)e_1$ with $W'(x^2) \geq 0$. The leading-order contribution to inertial particle velocity on the slow manifold (53) takes the form

$$v_p = (1-\alpha)\nabla^\perp \psi + \alpha W e_1 + \tau f_0((R-\alpha-1)\nabla \psi - \alpha W e_2) \quad (57)$$

with an $O(\text{Ro}^2)$ error. The divergence of this velocity,

$$\nabla \cdot v_p = \tau f_0((1-\alpha-R)\nabla^2 \psi - \alpha W'(x^2)). \quad (58)$$

Noting that both $1-\alpha-R$ and α are nonnegative, it follows that $\nabla \cdot v_p \leq 0$, which promotes attraction of inertial

particles toward the interior of the gyre in a manner akin to undrogued drifters and plastic debris.

A precise localization of the attractor can be attained by inspecting the streamfunction and the wind field. A simple expression for the streamfunction is⁷⁸

$$\psi = \frac{\pi F}{H\beta} \left(1 - x^1/L - e^{-\frac{x^1}{\tau/\beta}}\right) \sin \frac{\pi x^2}{L}, \quad (59)$$

where H is the (thermocline) depth, r is the (bottom) friction coefficient, L length of a square domain, and F is the wind stress (per unit density) amplitude, which sets the amplitude of the wind field:

$$W = \text{sign} \left(x^2 - \frac{1}{2}L\right) \sqrt{\frac{\rho F}{\rho_a C_D}} \sqrt{\text{sign} \left(\frac{1}{2}L - x^2\right) \cos \frac{\pi x^2}{L}}, \quad (60)$$

where C_D is a (dimensionless) drag coefficient. (We note that W is C^∞ everywhere except at $x^2 = \frac{1}{2}L$, a set of measure zero. Thus (57) is a valid approximation to (29) almost everywhere in the domain.) Figure 6 shows streamlines of $v = \nabla^\perp \psi$ on the left, $u = (1-\alpha)\nabla^\perp \psi + \alpha W e_1$ in the middle, and v_p given by (57) on the right. Parameters for the Stommel model are as in⁷⁷ with $C_D = 1.2 \times 10^{-379}$. Soft inertial parameters are chosen to represent undrogued GDP drifters, namely, $\delta = 2$ and $a = 17.5$ cm. We have set also $k = 1 = k_a$. The rest of the parameters are hard, typical seawater and air values. This gives $R = 0.6$ and $\tau = 0.0968$ d. Variations of the soft parameters do not change the qualitative aspects of the solution. The streamlines of v show a center, displaced westward, resulting from the β effect. The streamlines of u are similar, with a center in precisely the same place. This is located at $(x^1, x^2) = (-\frac{\tau}{\beta} \log \frac{\tau}{\beta L}, \frac{1}{2}L)$. The stability type of this equilibrium is changed to a *stable spiral* when the inertial velocity is v_p considered. (Indeed, we have numerically verified that, at that point, ∇v and ∇u both have complex conjugate pure imaginary eigenvalues, while the complex conjugate eigenvalue pair of ∇v_p has a negative real part.) This thus shows explicitly where inertial particles accumulate and further that finite-size effects, produced by the term proportional to τ in v_p , are responsible for driving the accumulation. A search-and-rescue type model, i.e., one for which $\dot{x} = u$ neglecting those effects, is not enough to realize it, as Beron-Vera, Olascoaga, and Lumpkin³⁵ noted earlier.

We finalize the Stommel model analysis by comparing the divergence of the inertial velocity (58) with that one that would result from the wind stress curl (Ekman divergence), namely,

$$\nabla \cdot v_E = -\frac{\pi F}{f_0 H L} \sin \frac{\pi x^2}{L}, \quad (61)$$

which is nonpositive. The comparison in presented in Figure 7. Note that $|\nabla \cdot v_p|$ dominates over $|\nabla \cdot v_E|$ in the domain (left panel) while both are much smaller than f_0 (right panel), reason for which the Ekman convergence does not enter in the Stommel model (its a higher-order

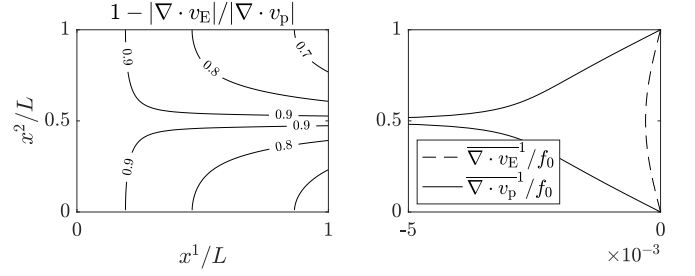


Figure 7. For the Stommel model, relative difference of inertial and Ekman divergence magnitudes (left) and zonally averaged inertial and Ekman divergences normalized by the Coriolis parameter (right).

effect in the Rossby number R_0). It is important to realize that the divergence $\nabla \cdot v_p / f_0$ at $x^2 = \frac{1}{2}L$ is not a deficiency of the Maxey–Riley description of inertial effects, but rather a consequence of the convenient form of the wind stress assumed by Stommel in his model, which leads to a divergence of the associated wind there.

We now proceed to test the ability of the Maxey–Riley set derived here to promote inertial particle concentration in the subtropical gyres in a realistic setting following Beron-Vera, Olascoaga, and Lumpkin³⁵. We focus on the North Atlantic for simplicity as subtropical gyres in the other oceans behave similarly. The exception is the Indian Ocean, where aggregation of inertial particles is not so evident, suggesting that ocean and atmospheric conditions are peculiar there⁸⁰. For instance, monsoon variability has been recently found to strongly constrain marine debris drift in that ocean²³.

Thus we feed the full spherical form of the Maxey–Riley set (A.6) with v as given by surface ocean velocity from the Global 1/12° HYCOM (HYbrid-Coordinate Ocean Model) + NCODA (Navy Coupled Ocean Data Assimilation) Ocean Reanalysis⁸¹, and v_a as the wind velocity from the National Centers for Environmental Prediction (NCEP) Climate Forecast System Reanalysis (CFSR) employed to construct the wind stress applied on the model. (To be more precise, the NCEP winds are provided at 10 m, so we multiply them by one half following Hsu, Meindl, and Gilhousen⁸² to infer v_a .) This way ocean currents and winds are made dynamically consistent with each other.

Specifically, we partition the North Atlantic domain into $5^\circ \times 5^\circ$ longitude–latitude boxes and construct a matrix of probabilities, P , of the drifters and the inertial particles to transitioning, irrespective of the start time, among them over a short time. Such a time-independent P represents a discrete autonomous transfer operator which governs the evolution of tracer probability densities, satisfying a stationary advection–diffusion process, on a Markov chain defined on the boxes of the partition^{23,83–86}. Thus given an initial probability vector \mathbf{f} , this is forward evolved under left multiplication by P , namely, $\mathbf{f}_n = \mathbf{f} P^n$, $n = 1, 2, \dots$. This way long-term evolution can be investigated in a probabilistic sense

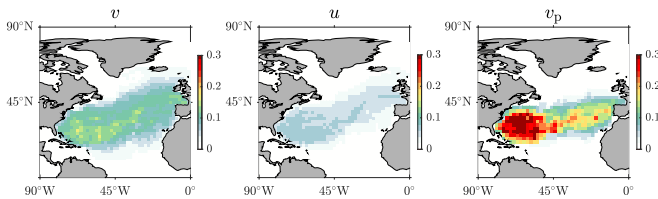


Figure 8. Long-term distribution in the North Atlantic of an initially uniform probability density under action of an autonomous transfer operator constructed using short-run trajectories produced by surface HyCOM velocity (left), δ -weighted velocity where seawater velocity is the HyCOM and the air velocity is the NCP wind used to force HyCOM (middle), and trajectories produced by the Maxey–Riley set derived in this paper fed with these seawater and air velocities (right). Soft inertial parameters choices are $\delta = 2$ and $a = 17.5$ cm, representing undrogued GDP drifters, and $k = 1 = k_a$. Densities are subjected to a sixth-root transformation

without the need of long trajectory records, which may be generated numerically but are not available from observations. To construct P we set a transition time of 5 days, which is longer than the Lagrangian decorrelation time scale, estimated to be of the order of 1 day near the ocean surface⁸⁷, thereby guaranteeing sufficiently negligible memory into the past that the Markov assumption can be expected to hold well.

Figure 8 shows distributions in the North Atlantic after 10 years of an initially uniform probability density evolving under the action of transition matrix constructed using trajectories produced by HyCOM surface ocean velocity output (left), trajectories of the δ -weighted velocity u resulting from setting v to be the HyCOM velocity and v_a to be the NCEP winds used to force the model (middle), and trajectories produced by the Maxey–Riley set fed with these velocities. (The full spherical form (A.6) of the set is employed in these calculations; trajectories of v and u are computed by integrating the left set in (A.3) with v_f replaced by v and u , respectively.) Parameters were taken as above to represent undrogued GDP drifters, $\delta = 2$ and $a = 17.5$ cm. Note the good qualitative agreement with the results based on the conceptual wind-driven circulation model of Stommel of Figure 6. Note the density values, which are subjected to a fourth-root transformation. Inertial particles reveal accumulation toward the center of the gyre, while seawater particles and particles evolving under the δ -weighted velocity u do not. Indeed, the densities corresponding to the latter are low and distributed more homogeneously over the gyre. Garbage patches in the ocean tend to localize in the center of the gyres consistent with the inertial particles. These reinforces the idea put forth by Beron-Vera, Olascoaga, and Lumpkin³⁵ that inertial effects dominate the production of such patches. Ekman transport convergence, the only mechanism acting in the absence of inertial effects, does not control garbage accumulation despite earlier⁸⁸ and recent⁸⁰ claims. Further-

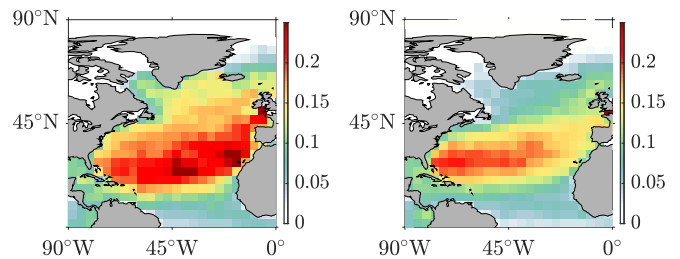


Figure 9. Long-term distribution in the North Atlantic of an initially uniform probability density under action of an autonomous transfer operator constructed using short-run drogued (left) and undrogued (right) trajectories of satellite-tracked drifting buoys from the NOAA Global Drifter Program. Densities are subjected to a fourth-root transformation

more, ignoring finite-size effects results in strong dispersion by view of the very low density values attained. This questions the validity of the leeway modeling framework. The results based on the slow manifold reduction of the Maxey–Riley set are indistinguishable from those based on the full set, which was v -initialized with mean HyCOM velocity. This provides support for the validity of the slow manifold reduction.

Finally, Figure 9 shows the distribution of an initially uniform probability density after 10 years of forward evolution under a discrete action of a transfer operator constructed using drogued (left) and undrogued (right) drifter trajectories from the GDP dataset. Note how undrogued drifter density in the long run tends to concentrate in the center of the gyre more evidently than drogued drifter density. Such a difference was not noted in previous work^{88,89} which also used probabilistic approaches to investigate long-term behavior. Very importantly, note that this behavior resembles quite well the simulated behavior described above, providing a reality check for it. More specifically, the drogued drifters behave in manner akin to seawater particles. The undrogued drifters, by contrast, behave more like inertial particles, which represent a prototype for flotsam in general as undrogued drifters and plastic debris present a similar tendency to aggregate in the interior of the subtropical gyres.

VI. DISCUSSION

A. Shape corrections

The Maxey–Riley theory for inertial ocean dynamics proposed in this paper has several limitations. First is its restriction to spherical particles (objects), which constrains its ability to account for the motion of marine debris in general.

Posing the general problem of a rigid body of arbitrary shape moving in the flow of a fluid is a very difficult task, which is beyond the scope of our paper. However, we

propose a heuristic fix that can be expected to be valid for sufficiently small objects, following work by Ganser⁹⁰. In that work, a simple a shape factor, K , depending on geometric shape descriptors' sphericity and the projected area in the motion direction, is considered to model the drag coefficient for nonspherical particles.

Recall first that the drag force⁶¹

$$F_{\text{drag}} = \frac{1}{2} \rho_f C_D A_f |v_f - v_p| (v_f - v_p) \quad (62)$$

A particle in a flow in Stokes' regime, for which $\text{Re}_p = \frac{|v_f - v_p| \ell_f}{\mu_f / \rho_f} < 1$, is characterized by a drag coefficient

$$C_D = \frac{24}{\text{Re}_p}. \quad (63)$$

This leads to the Stokes law for drag, i.e., formula (17) multiplied by m_p .

Ganser⁹⁰ proposes, following earlier work by others (cf. references cited by Ganser), to correct the drag coefficient for particle shape by replacing C_D by $C_D \cdot K^{-1}$, where

$$K^{-1} = \frac{1}{3} \frac{d_n}{d_v} + \frac{2}{3} \frac{d_s}{d_v}. \quad (64)$$

Here d_n is the diameter of the sphere with equivalent projected area, d_s is the diameter of the sphere with equivalent surface area, and d_v is diameter of the sphere with equivalent volume. For a sphere of radius a , $d_n = d_s = d_v = 2a$, which gives $K = 1$ so no shape correction is needed in that case as expected. But for example for the case of a cube of side l , one computes $d_n = 2l \sqrt[3]{3/4\pi}$, $d_s = l\sqrt{6\pi}$, and $d_v = 2l/\sqrt{\pi}$, which gives $K \approx 0.95$, implying a smaller drag relative to an equivalent sphere.

The above thus provides a simple heuristic means adapt the Maxey–Riley set derived here to be valid for small particles that deviate from spherical. To wit, just replace τ in (28) by $\tau \cdot K$ with the appropriate K . A caveat is that K is nonunique for nonisometric shapes owing to orientation dependence. If the nonisometric particle is in Stokes' regime and the *orientation* is known, so the projected area can be computed, the value of K given by (64) should be used. If the orientation is not known, Ganser⁹⁰ recommends to use *the average of the two extreme values of K* .

B. Stokes drift

The Maxey–Riley set derived here assumed a flat air–sea interface, which can result in inadequate modeling of drift in the presence of waves. Wave-induced Stokes drift generates Langmuir cells, which are thought to be a controlling factor in the ocean's uppermost layer⁹¹. Stokes drift has been reported to cause objects to move at a faster speed than would be predicted using the surface currents in the SAR literature^{16,57,92}.

A first step toward including Stokes drift effects is at the level of the carrying flow. The Stokes drift arises

due to material orbits not being closed under a wavy water surface⁹³. As a Lagrangian quantity (i.e., fluid particle following), it cannot be represented in conventional ocean circulation models that use an Eulerian description⁹⁴. Coupled ocean–wave circulation models can provide the required Stokes drift representation through Stokes–Coriolis forcing on the mean flow due to the interaction of the wave-induced Stokes drift and the Coriolis effect⁹⁵. In these models the waves affect the mean ocean flow, which itself affects the waves through advection, refraction, and wave blocking. However, coupled ocean–wave modeling is challenging, particularly in long integrations (weeks to months) as the ocean component will tend to drift without data assimilation⁹⁶.

A suboptimal, yet more feasible, approach is to add the Stokes drift a posteriori on the mean ocean velocity, assuming that waves do not affect the mean ocean dynamics. Denoting the Stokes drift velocity by v_S and the Eulerian velocity output from an ocean model by v_E (representing the barotropic and baroclinic ocean circulation on time scales considerably longer than the surface gravity wave period) it is customary to write⁹⁷

$$v = v_E + v_S. \quad (65)$$

If the directional wave spectrum, $E(\omega, \theta)$ where ω is frequency and θ propagation direction, is available from a numerical wave prediction model, whether forced by the mean ocean dynamics or not, then correct to second order in the wave steepness, the Stokes drift velocity in deep water can be written as⁹⁸

$$v_S(z) = 2 \int \omega k e^{2|\mathbf{k}|z} E(\omega, \theta) d\omega d\theta, \quad (66)$$

where \mathbf{k} is wavenumber. The magnitude and vertical shear of the Stokes drift depends on the wave conditions. Young wind sea with predominantly short waves results in fast surface Stokes drift and strong vertical shear, while long period swell produces a slower Stokes drift that is more uniformly distributed with depth. For small spheres vertical shear effects may be ignored in both situations.

When full wave spectra are not available, which is usually the case, simplifications are considered. For instance, assuming that wind and waves are aligned and that the wave field is in a steady state, Wu⁹⁹ proposes the following parameterization for the Stokes drift at the surface of the ocean:

$$v_S = 0.0186 \cdot (gL_{\text{fetch}} v_{10}^{-2})^{0.03} v_{10}, \quad (67)$$

where L_{fetch} is wave fetch, and v_{10} is wind velocity at 10 m. While wind velocity is readily available from models or reanalyses, wave fetch is difficult to quantify in the field where there is directional spread. Parameterizations that depend on bulk wave parameters such as significant wave height (H_s) and peak wave period (T_p) and direction (θ_p) are more useful in practice. For instance, Tamura, Miyazawa, and Oey¹⁰⁰ propose

$$v_S = \pi^3 g^{-1} H_s^2 T_p^{-3} (\cos \theta_p, \sin \theta_p), \quad (68)$$

where g is gravity. Further parameterizations along related lines have been proposed in the literature^{101–103}.

C. Memory effects

If the particle velocity differs than the carrying fluid velocity at the initial time, then the acceleration produced by the Basset–Boussinesq memory term is⁴⁹

$$F_{\text{mem}} = \frac{6\sqrt{\mu_f \rho_f} A_f}{m_p} \cdot (v_f - v_p)^{(1/2)}, \quad (69)$$

where

$$w^{(1/2)} := \frac{1}{\sqrt{\pi}} \frac{d}{dt} \int_{t_0}^t \frac{w(s)}{\sqrt{t-s}} ds \quad (70)$$

with $t \geq t_0$ is a Riemann–Liouville-type fractional derivative for the function $w(t)$. This term has been neglected here under long recurrence time grounds. This is cannot be expected to a priori hold within Lagrangian vortices of the type discussed above. Thus for completeness we present the correction to the Maxey–Riley set (29) needed to account for memory effects.

Applying on (69) the same procedure applied on the rest of the forces involved in the Maxey–Riley equation, the resulting correction is a term to be added to the right-hand-side of (29), which given by

$$\frac{\langle F_{\text{mem}} \rangle}{\frac{3}{2} (1 - \frac{1}{6} \Phi)} \stackrel{\rho_a \ll \rho}{=} \frac{\tilde{R}}{\sqrt{\tau}} (v - v_p)^{(1/2)}, \quad (71)$$

where

$$\tilde{R} := \frac{\pi \sqrt{3\delta(2 - \Phi)(1 - \Psi)}}{\sqrt{1 - \frac{1}{6} \Phi} \sqrt{k^{-1}(1 - \Psi) + k_a^{-1} \gamma \Psi}}. \quad (72)$$

Unfortunately, the term above will not convey the Maxey–Riley set with the original set's behavior when memory effects are taken into account⁴⁷. To wit, that v_p decays algebraically in time to a limit that is $O(\tau)$ -close to the carrying flow velocity, which in our surface ocean dynamics context is effectively given by u . To conserve that behavior, $u - v_p$ should appear in the memory term instead of $v - v_p$. With this in mind, we heuristically propose to make

$$\frac{\langle F_{\text{mem}} \rangle}{\frac{3}{2} (1 - \frac{1}{6} \Phi)} \mapsto \frac{\tilde{R}}{\sqrt{\tau}} (u - v_p)^{(1/2)}, \quad (73)$$

so the Maxey–Riley set with memory reads

$$\begin{aligned} \dot{v}_p + \left(f + \frac{1}{3} R\omega\right) v_p^\perp + \tau^{-1} v_p + \tilde{R} \tau^{-1/2} v_p^{(1/2)} \\ = R \frac{Dv}{Dt} + R \left(f + \frac{1}{3} \omega\right) v^\perp + \tau^{-1} u + \tilde{R} \tau^{-1/2} u^{(1/2)}, \end{aligned} \quad (74)$$

for some $\tilde{R}(\delta)$ to be determined from numerical experimentation in front of observations. This task and the formal verification that the results of Langlois, Farazmand, and Haller⁴⁷ translate *mutatis mutandis* are deferred to the future. We note that numerical integration of (74) cannot be carried out using a standard Runge–Kutta method. Rather, a specialized method^{45,104} is required.

D. Density inhomogeneities

Finally, ignoring lateral gradients and temporal variations of the density of the advecting fluid can be consequential, particularly near frontal regions. While the original Maxey–Riley set was derived for the case of homogeneous carrying fluid density, heuristic extensions to the inhomogeneous case have been proposed¹⁰⁵, which can be considered. More specifically, Tanga and Provenzale¹⁰⁵ considered the motion of particles in a stable stratified fluid with buoyancy oscillating around a reference density as an idealized representation of the motion of an atmospheric balloon or an oceanic subsurface buoy (float). This translated into making parameter δ in the original Maxey–Riley set (Tanga and Provenzale¹⁰⁵ did not consider planet's rotation and sphericity effects) a periodic function of time by making ρ_p a periodic function of time which keeping ρ constant. These authors found that by allowing δ to vary with time, the motion of inertial particles may be chaotic even though the fluid (or, equivalently, the non-oscillating) particles undergo regular motion and follow the streamlines of the Eulerian flow.

The above heuristics may be modified to investigate the situation in which an inertial particle with fixed density ρ_p moves through an ambient fluid whose density ρ changes in space and time. This corresponds to making δ a predefined arbitrary function of x and t . In our case, ρ is the density of the seawater. The air density does not appear in the Maxey–Riley set (29). Indeed, the only air parameter is the air viscosity, which can be kept safely fixed. The condition $\delta(x, t) \geq 1$ needed for the Maxey–Riley set to remain valid should not be difficult to be satisfied for an initially sufficiently buoyant particle given that the change of ρ across the sharpest fronts does not exceed a few percent¹⁰⁶. Such small a change in δ can still impact the trajectory of an inertial particle by view of the results of Tanga and Provenzale¹⁰⁵.

Taking the resulting Maxey–Riley set as formally valid with the above modification, its slow manifold reduction will still be given by (53). In order to compute it, however, one must remove from τ any function depending on δ so it can be taken as a fixed (small) perturbation parameter.

VII. CONCLUDING REMARKS

In this paper we have proposed a theory for the motion finite-size particles floating at the ocean surface based on the Maxey–Riley set, the de-jure fluid dynamics framework for inertial particle motion investigation. The theory thus consist of a Maxey–Riley set obtained by vertically averaging the various forces involved in the original Maxey–Riley set, appropriately adapted to account for planet’s rotation and sphericity effects, across an assumed small spherical particle that floats at a flat air–sea interface and thus is subjected to the action ocean currents and winds.

The inertial particle velocity of the resulting Maxey–Riley set is shown decay exponentially fast in time to a limit that is $O(a^2)$ -close, where a is the particle radius, to an average of the seawater and air velocities weighted by a function of the seawater-to-particle density ratio. This weighted average velocity has a form which is similar to the so-called leeway velocity that forms the basis for search-and-rescue modeling. Such a leeway model is not sufficient to explain the role of mesoscale eddies as traps for marine debris or the formation of garbage patches in subtropical gyres, which are phenomena dominated by finite-size effects.

The resulting Maxey–Riley set either outperforms or has potential for outperforming an earlier proposed set³⁵ in various aspects. For instance, in the neutrally buoyant case, inertial particle motion is synchronized with seawater (i.e., Lagrangian) particle motion under the same conditions as in the original Maxey–Riley set without Coriolis and lift forces. Also, the newly proposed set predicts concentration of particles inside anticyclonic mesoscale eddies consistent with observations of marine microplastic debris. On the other hand, including lift force force the new Maxey–Riley set is expected to better represent particle dispersion in the presence of fast submesoscale eddy motion. Furthermore, the proposed heuristic shape corrections raise the earlier set limitation to spherical particles. Finally, recommendations were made for accounting for Stokes drift effects are expected to improve the earlier set performance in the presence of waves, and proposals for including memory effects to improve its ability to simulate inertial particle dynamics in the presence of recurrent motions and also for incorporating the effects of inhomogeneities of the carrying density field, which can be consequential near frontal regions.

We close by noting that a paper in preparation³⁹ reports on the results from a field experiment which involved the deployment, in the Gulf Stream and other areas of the North Atlantic, and subsequently tracking, using global satellite positioning, of buoys of varied buoyancies, sizes, and shapes. In that paper the Maxey–Riley set derived here is shown capable of reproducing individual trajectories with unexpected accuracy given the uncertainty around the ocean current and wind representations, providing strong support the validity of the set.

ACKNOWLEDGMENTS

The Blended Sea Winds data employed in this paper are available from NOAA/NCDC (<http://ncdc.noaa.gov>). The altimeter products were produced by SSALTO/DUCAS and distributed by AVISO with support from CNES (<http://www.aviso.oceanobs>). The drifter data were collected by the NOAA Global Drifter Program (<http://www.aoml.noaa.gov/phod/dac>). The $1/12^\circ$ Global HYCOM+NCODA Ocean Reanalysis was funded by the U.S. Navy and the Modeling and Simulation Coordination Office. Computer time was made available by the DoD High Performance Computing Modernization Program. The output and forcing are publicly available at <http://hycom.org>. Our work was supported by the University of Miami’s Cooperative Institute for Marine & Atmospheric Studies (CIMA).

Appendix A: Inertial ocean dynamics on the sphere

Let a_\odot be the mean radius of the Earth, and consider the rescaled longitude (λ) and latitude (ϑ) coordinates, namely,

$$x^1 = (\lambda - \lambda_0) \cdot a_\odot \cos \vartheta_0, \quad x^2 = (\vartheta - \vartheta_0) \cdot a_\odot, \quad (\text{A.1})$$

respectively, measured from an arbitrary location on the surface of the planet. Consider further the following geometric coefficients⁵³:

$$\gamma_\odot := \sec \vartheta_0 \cos \vartheta, \quad \tau_\odot := a_\odot^{-1} \tan \vartheta. \quad (\text{A.2})$$

The (horizontal) velocity of a fluid particle and its acceleration as measured by a terrestrial observer are^{53,107}

$$v_f = \begin{pmatrix} \gamma_\odot & 0 \\ 0 & 1 \end{pmatrix} \dot{x}, \quad a_f = \dot{v}_f + (f + \tau_\odot v_f^1) v_f^\perp, \quad (\text{A.3})$$

respectively, where $f = 2\Omega \sin \vartheta$. It is important to realize that this is not a mere change of coordinates from Cartesian to spherical. Very differently, this is a consequence of the gravitational force, which, attracting the particle to the nearest pole, is required to sustain a steady rotation, with angular velocity $\pm\Omega$, relative to a fixed frame, at any point on the planet’s surface. The terrestrial observer is then left with *just* the Coriolis force, in the absence of any other forces, to describe motion on the surface of the Earth. A very enlightening way to derive the formula for the acceleration in (A.3) is from Hamilton’s principle, with the Lagrangian as written by an observer standing in a fixed frame, so the only force acting on the particle (in the absence of any other forces) is the gravitational one, and the coordinates employed by this observer related to those rotating with the planet (A.1)^{53,107}. This is in essence what Pierre Simon de Laplace (1749–1827) did to derive his theory of tides and at the same time discover the Coriolis force over a quarter

of a century before Gaspard Gustave de Coriolis (1792–1843) was born¹⁰⁸. For a nice account on the history of this, many times misunderstood, force, cf. Ripa¹⁰⁹.

By a similar token, the fluid's Eulerian acceleration takes the form

$$\frac{Dv_f}{Dt} + (f + \tau_\odot v_f^1) v_f^\perp, \quad (\text{A.4})$$

where

$$\frac{Dv_f}{Dt} = \partial_t v_f + (\nabla v_f) \dot{x} = \partial_t v_f + (\gamma_\odot^{-1} \partial_1 v_f) v_f^1 + (\partial_2 v_f) v_f^2. \quad (\text{A.5})$$

Equations hold for a particle of fluid, either seawater or air, and also for an inertial particle. The acceleration of the inertial particle on the left-hand-side of (yet to be evaluated) Maxey–Riley set (21) and in the added mass force (14) is the β -plane form of a_f in (A.3) for the case of an inertial particle, resulting from making $\gamma_\odot = 1$, $\tau_\odot = 0$, and $f = f_0 + \beta x^2$, which, despite its wide used, does not represent a consistent leading order in $|x^2|/a_\odot \ll 1$ approximation⁵³. In turn, the fluid's Eulerian acceleration that appear in the flow force (13) and the added mass term (14) is the β -plane form of (A.4)–(A.5).

With the above in mind, the Maxey–Riley set (29) on the sphere then takes the form

$$\begin{aligned} \dot{v}_p + (f + \tau_\odot v_p^1 + \tfrac{1}{3} R\omega) v_p^\perp + \tau^{-1} v_p \\ = R \frac{Dv}{Dt} + R (f + \tau_\odot v^1 + \tfrac{1}{3} \omega) v^\perp + \tau^{-1} u, \end{aligned} \quad (\text{A.6})$$

with $\frac{Dv}{Dt}$ given by (A.5) and

$$\omega = \gamma_\odot^{-1} \partial_1 v^2 - \gamma_\odot^{-1} \partial_2 (\gamma_\odot v^1) = \gamma_\odot^{-1} \partial_1 v^2 - \partial_2 v^1 + \tau_\odot v^1 \quad (\text{A.7})$$

as it follows from its definition, $\omega := \lim_{\Delta x^1 \Delta x^2 \rightarrow 0} \frac{1}{\gamma_\odot \Delta x^1 \Delta x^2} \oint (\gamma_\odot v^1 dx^1 + v^2 dx^2)$, and noting that $\gamma_\odot(x^2)/\gamma_\odot(x^2) = -\tau_\odot(x^2)$

Applying the slow-manifold reduction on (A.6) it follows, to leading order on the slow manifold, that

$$\begin{aligned} \dot{x} \sim u + \tau \left(R \frac{Dv}{Dt} + R (f + \tau_\odot v^1 + \tfrac{1}{3} \omega) v^\perp \right. \\ \left. - \frac{Du}{Dt} - (f + \tau_\odot v^1 + \tfrac{1}{3} R\omega) u^\perp \right), \end{aligned} \quad (\text{A.8})$$

where $\frac{D}{Dt}u$ is as in (A.5) with v_f replaced by u .

Appendix B: Attractivity and instability conditions for neutrally buoyant particles

To derive an attractivity condition for \mathcal{N} in the present geophysical setting ($f \neq 0$) with lift force, we follow Sapsis and Haller⁶³ closely by first fixing a solution $(y, x)(t)$ to (33), which fixes $A(x(t), t)$. Then noting that

$y^\top A y = y^\top (rA + (1-r)A^\top) y$ for any $r \in \mathbb{R}$, one finds, using $r = \frac{1}{2}$, that $y^\top A y \leq \max \text{spec} \frac{A+A^\top}{2} \cdot |y|^2$, which follows from real symmetric $A + A^\top$ admitting an orthogonal diagonalization. Now, taking into account that $J = -J^\top$,

$$\frac{A + A^\top}{2} = S + \tau^{-1} \text{Id} \quad (\text{B.1})$$

and hence

$$\frac{1}{2} \frac{d}{dt} |y|^2 = -y^\top (S + \tau^{-1} \text{Id}) y \leq -\min \text{spec}(S + \tau^{-1} \text{Id}) \cdot |y|^2. \quad (\text{B.2})$$

Integrating from $t = t_0$ to $t > t_0$,

$$|y(t)|^2 \leq |y(t_0)|^2 e^{-\int_{t_0}^t (S(x(s), s) + \tau^{-1} \text{Id}) ds}. \quad (\text{B.3})$$

Then for $|y(t)|$ to decay from $|y(t_0)|$ as t increases, the integrand in (B.3) must be positive for all $x \in D$ over the time interval I , from which the global attractivity condition (35) follows.

As noted by Sapsis and Haller⁶³, perturbations off \mathcal{N} which are initially sufficiently small will grow or decay depending on the sign of the instantaneous stability indicator

$$\Lambda(x_0, t_0) = \lim_{t \rightarrow t_0} \frac{2}{t - t_0} \log \|P_{t_0}^t\|_2 \quad (\text{B.4})$$

Here $P_{t_0}^t$ satisfies

$$\dot{P}_{t_0}^t = A(x(t; t_0, x_0), t) P_{t_0}^t, \quad P_{t_0}^{t_0} = \text{Id}, \quad (\text{B.5})$$

so $y(t; t_0, y_0, x_0) = P_{t_0}^t y_0$, to wit, $P_{t_0}^t$ represents the fundamental matrix solution of (33) for initial condition $(y, x)(t_0) = (y_0, x_0)$. Taylor expanding $P_{t_0}^t$ one finds

$$P_{t_0}^t = \text{Id} + A_0 \cdot (t - t_0) + O((t - t_0)^2), \quad (\text{B.6})$$

where the shorthand notation $A_0 = A(t_0)$ is used, and hence

$$(P_{t_0}^t)^\top P_{t_0}^t = \text{Id} + (A_0 + A_0^\top) \cdot (t - t_0) + O((t - t_0)^2). \quad (\text{B.7})$$

Then

$$(\|P_{t_0}^t\|_2)^2 = 1 - 2 \min \text{spec}(S_0 + \tau^{-1} \text{Id}) \cdot (t - t_0) + O((t - t_0)^2), \quad (\text{B.8})$$

where (B.1) was used. Now, using $\log(1 + \sum_1^\infty c_n \varepsilon^n) = c_1 \varepsilon + O(\varepsilon^2)$ for $\varepsilon > 0$ small, one finds

$$\Lambda(x_0, t_0) = -2 \min \text{spec}(S(x_0, t_0) + \tau^{-1} \text{Id}). \quad (\text{B.9})$$

Replacing (x_0, t_0) with $(x(t), t)$, it follows that instantaneous divergence away from \mathcal{N} will take place where $S + \tau^{-1} \text{Id}$ is sign indefinite, or, equivalently, where (35) is violated.

Appendix C: Slow manifold reduction in the standard fluid mechanics setting with lift force

The standard fluid mechanics Maxey–Riley equation with lift force is given by⁴³ (Chapter 4)

$$\dot{v}_p + \frac{1}{2}R\omega v_p^\perp + \tau^{-1}v_p = \frac{3}{2}R\frac{Dv}{Dt} + \frac{1}{2}R\omega v^\perp + \tau^{-1}v, \quad (C.1)$$

where v is any carrying flow velocity and

$$\tau := \frac{2R}{9} \cdot \frac{a^2}{\mu/\rho}, \quad R := \frac{2\delta}{2 + \delta}. \quad (C.2)$$

In nondimensional variables with time rescaled as in §4, the above equation in system form reads

$$x' = \tau v_p, \quad (C.3)$$

$$\varphi' = \tau, \quad (C.4)$$

$$v'_p = v - v_p - \frac{1}{2}\tau R\omega v_p^\perp + \frac{3}{2}\tau R\frac{Dv}{Dt} + \frac{1}{2}\tau R\omega v^\perp. \quad (C.5)$$

Solutions of the $\tau = 0$ limit of the above set are easily seen to be attracted by

$$\mathcal{S}_0 = \{(x, \varphi, v_p) \mid v_p = v(x, \varphi), x \in D, \varphi \in I\}. \quad (C.6)$$

This indicates that the slow manifold has the following Taylor expansion:

$$\begin{aligned} \mathcal{S}_\tau := \{(x, \varphi, v_p) \mid v_p = v(x, \varphi) + \sum_{n=1}^r \tau^n v_n(x, \varphi) \\ + O(\tau^{r+1}), (x, \varphi) \in D \times I\}. \end{aligned} \quad (C.7)$$

Differentiating the above one gets (48) with u replaced by v . Then restricting (C.5) to \mathcal{S}_τ , i.e.,

$$\begin{aligned} v'_p &= \left[v - v_p - \frac{1}{2}\tau R\omega v_p^\perp + \frac{3}{2}\tau R\frac{Dv}{Dt} + \frac{1}{2}\tau R\omega v^\perp \right]_{\mathcal{S}_\tau} \\ &= - \sum_{n=1}^r \tau^n v_n - \frac{1}{2}\tau R\omega \left(v^\perp + \sum_{n=1}^r \tau^n v_n^\perp \right) + \frac{3}{2}\tau R\frac{Dv}{Dt} \\ &\quad + \frac{1}{2}\tau R\omega v^\perp + O(\tau^{r+2}), \end{aligned} \quad (C.8)$$

and equating equal τ -power terms (48) with u replaced by v and (C.8), we obtain

$$v_1 = \left(\frac{3}{2}R - 1 \right) \frac{Dv}{Dt} \quad (C.9)$$

$$\begin{aligned} v_n &= -\frac{1}{2}R\omega v_{n-1}^\perp \\ &\quad - \partial_t u_{n-1} - (\nabla v_{n-1})v - (\nabla v)v_{n-1} \\ &\quad - \sum_{m=1}^{n-2} (\nabla v_m)v_{n-m-1}, \quad n \geq 2. \end{aligned} \quad (C.10)$$

The Maxey–Riley set (C.1) on the slow manifold \mathcal{S}_τ reduces to

$$\dot{x} = v_p = v(x, t) + \sum_{n=1}^r \tau^n v_n(x, t) + O(\tau^{r+1}) \quad (C.11)$$

with $v_n(x, t)$ as given in (C.9)–(C.10). Note that the lift force makes an $O(\tau^2)$ contribution to \mathcal{S}_τ .

REFERENCES

- ¹G. G. Stokes, “On the Effect of the Internal Friction of Fluids on the Motion of Pendulums,” *Transactions of the Cambridge Philosophical Society* **9**, 8 (1851).
- ²A. B. Basset, “Treatise on hydrodynamics,” (Deighton Bell, London, 1888) Chap. 22, pp. 285–297.
- ³J. V. Boussinesq, “Sur la résistance qu’oppose un fluide indéfini au repos, sans pesanteur, au mouvement varié d’une sphère solide qu’il mouille sur toute sa surface, quand les vitesses restent bien continues et assez faibles pour que leurs carrés et produits soient négligeables,” *Comptes Rendu de l’Academie des Sciences* **100**, 935–937 (1885).
- ⁴C. W. Oseen, *Hydrodynamik* (Akademische Verlagsgesellschaft, Leipzig, 1927).
- ⁵C. M. Tchen, Ph.D. thesis, Delft, Martinus Nijhoff, The Hage (1947).
- ⁶S. Corrsin and J. Lumely, *Appl. Sci. Res. A* **6**, 114 (1956).
- ⁷M. R. Maxey and J. J. Riley, “Equation of motion for a small rigid sphere in a nonuniform flow,” *Phys. Fluids* **26**, 883 (1983).
- ⁸J. J. Riley, Ph.D. thesis, The John Hopkins University, Baltimore, Maryland (1971).
- ⁹R. Gatignol, “The faxen formulae for a rigid particle in an unsteady non-uniform stokes flow,” *J. Mec. Theor. Appl.* **1**, 143–160 (1983).
- ¹⁰T. R. Auton, F. C. R. Hunt, and M. Prud’homme, “The force exerted on a body in inviscid unsteady non-uniform rotational flow,” *J. Fluid. Mech.* **197**, 241 (1988).
- ¹¹E. E. Michaelides, “Review—The transient equation of motion for particles, bubbles and droplets,” *ASME. J. Fluids Eng.* **119**, 233–247 (1997).
- ¹²A. Provenzale, “Transport by coherent barotropic vortices,” *Annu. Rev. Fluid Mech.* **31**, 55–93 (1999).
- ¹³J. H. E. Cartwright, U. Feudel, G. Károlyi, A. de Moura, O. Piro, and T. Tél, “Dynamics of finite-size particles in chaotic fluid flows,” in *Nonlinear Dynamics and Chaos: Advances and Perspectives*, edited by M. Thiel et al. (Springer-Verlag Berlin Heidelberg, 2010) pp. 51–87.
- ¹⁴A. Babiano, J. H. Cartwright, O. Piro, and A. Provenzale, “Dynamics of a small neutrally buoyant sphere in a fluid and targeting in Hamiltonian systems,” *Phys. Rev. Lett.* **84**, 5,764–5,767 (2000).
- ¹⁵R. D. Vilela, A. P. S. de Moura, and C. Grebogi, “Finite-size effects on open chaotic advection,” *Phys. Rev. E* **73**, 026302 (2006).
- ¹⁶Ø. Breivik, A. A. Allen, C. Maisondieu, and M. Olagnon, “Advances in search and rescue at sea,” *Ocean Dynamics* **63**, 83–88 (2013).
- ¹⁷L. Bellomo, A. Griffo, S. Cosoli, P. Falco, R. Gerin, I. Iermano, A. Kalampokis, Z. Kokkini, A. Lana, M. Magaldi, I. Mamoutos, C. Mantovani, J. Marmain, E. Potiris, J. Sayol, Y. Barbin, M. Berta, M. Borghini, A. Bussani, L. Corgnati, Q. Dagneaux, J. Gaggelli, P. Guterman, D. Mallarino, A. Mazzoldi, A. Molcard, A. Orfila, P.-M. Poulain, C. Quentin, J. Tintoré, M. Utieri, A. Vetrano, E. Zambianchi, and V. Zervakis, “Toward an integrated hf radar network in the mediterranean sea to improve search and rescue and oil spill response: the toasca project experience,” *Journal of Operational Oceanography* **8**, 95–107 (2015).
- ¹⁸J. Gower and S. King, “Satellite images show the Movement of floating *Sargassum* in the Gulf of Mexico and Atlantic Ocean,” Available from Nature Precedings (<http://hdl.handle.net/10101/npre.2008.1894.1>) (2008).
- ¹⁹M. T. Brooks, V. J. Coles, and W. C. Coles, “Inertia influences pelagic *sargassum* advection and distribution,” *Geophysical Research Letters* **46**, 2610–2618 (2019).
- ²⁰K. L. Law, S. Morét-Ferguson, N. A. Maximenko, G. Proskurowski, E. E. Peacock, J. Hafner, and C. M. Reddy, “Plastic accumulation in the North Atlantic subtropical gyre,” *Science* **329**, 1185–1188 (2010).

- ²¹A. Cozar, F. Echevarria, J. I. Gonzalez-Gordillo, X. Irigoien, B. Ubeda, S. Hernandez-Leon, A. T. Palma, S. Navarro, J. Garcia-de Lomas, R. andrea, M. L. Fernandez-de Puelles, and C. M. Duarte, "Plastic debris in the open ocean," *Proc. Nat. Acad. Sci. USA* **111**, 10239–10244 (2014).
- ²²J. A. Trinanés, M. J. Olascoaga, G. J. Goni, N. A. Maximenko, D. A. Griffin, and J. Hafner, "Analysis of flight MH370 potential debris trajectories using ocean observations and numerical model results," *Journal of Operational Oceanography* **9**, 126–138 (2016).
- ²³P. Miron, F. J. Beron-Vera, M. J. Olascoaga, and P. Koltai, "Markov-chain-inspired search for MH370," *Chaos: An Interdisciplinary Journal of Nonlinear Science* **29**, 041105 (2019).
- ²⁴I. Rypina, S. R. Jayne, S. Yoshida, A. M. Macdonald, E. Douglas, and K. Buesseler, "Short-term dispersal of Fukushima-derived radionuclides off Japan: modeling efforts and model-data intercomparison," *Biogeosciences* **10**, 4973–4990 (2013).
- ²⁵J. P. Matthews, L. Ostrovsky, Y. Yoshikawa, S. Komori, and H. Tamura, "Dynamics and early post-tsunami evolution of floating marine debris near Fukushima Daiichi," *Nature Geosci.* **10**, 598–603 (2017).
- ²⁶S. Szanyi, J. V. Lukovich, and D. G. Barber, "Lagrangian analysis of sea-ice dynamics in the arctic ocean," *Polar Research* **35**, 30778 (2016).
- ²⁷P. Nielsen, "Suspended sediment particle motion in coastal flows," *Coastal Engineering Proceedings* **1**, 2406–2416 (1994).
- ²⁸R. Reigada, R. M. Hillary, M. A. Bees, J. M. Sancho, and F. Sagues, "Plankton blooms induced by turbulent flows," *Proc. R. Soc. B: Biological Sciences* **270**, 875–880 (2003).
- ²⁹J. Peng and J. O. Dabiri, "Transport of inertial particles by Lagrangian Coherent Structures: application to predator-prey interaction in jellyfish feeding," *J. Fluid Mech.* **623**, 75–84 (2009).
- ³⁰P. Monroy, E. Hernández-García, V. Rossi, and C. López, "Modeling the dynamical sinking of biogenic particles in oceanic flow," (2016).
- ³¹F. J. Beron-Vera, M. J. Olascoaga, G. Haller, M. Farazmand, J. Triñanes, and Y. Wang, "Dissipative inertial transport patterns near coherent Lagrangian eddies in the ocean," *Chaos* **25**, 087412 (2015).
- ³²G. Haller and F. J. Beron-Vera, "Coherent Lagrangian vortices: The black holes of turbulence," *J. Fluid Mech.* **731**, R4 (2013).
- ³³G. Haller and F. J. Beron-Vera, "Addendum to 'Coherent Lagrangian vortices: The black holes of turbulence'," *J. Fluid Mech.* **755**, R3 (2014).
- ³⁴G. Haller, A. Hadjighasem, M. Farazmand, and F. Huhn, "Defining coherent vortices objectively from the vorticity," *J. Fluid Mech.* **795**, 136–173 (2016).
- ³⁵F. J. Beron-Vera, M. J. Olascoaga, and R. Lumpkin, "Inertia-induced accumulation of flotsam in the subtropical gyres," *Geophys. Res. Lett.* **43**, 12228–12233 (2016).
- ³⁶N. A. Maximenko and P. P. Niiler, "Mean surface circulation of the global ocean inferred from satellite altimeter and drifter data," in *15 years of Progress in Radar Altimetry* (ESA Publication SP-614, 2006).
- ³⁷L. Brach, P. Deixonne, M.-F. Bernard, E. Durand, M.-C. Desjean, E. Perez, E. van Sebille, and A. ter Halle, "Anticyclonic eddies increase accumulation of microplastic in the north atlantic subtropical gyre," *Marine Pollution Bulletin* **126**, 191–196 (2018).
- ³⁸D. B. Chelton, P. Gaube, M. G. Schlax, J. J. Early, and R. M. Samelson, "The influence of nonlinear mesoscale eddies on near-surface oceanic chlorophyll," *Science* **334**, 328–332 (2011).
- ³⁹M. J. Olascoaga, F. J. Beron-Vera, P. Miron, R. Lumpkin, J. Trinanés, and G. J. Goni, "Building a Maxey–Riley framework for inertial ocean dynamics. Part II: Field testing," In preparation. (2019).
- ⁴⁰While having a positive discriminant, the cubic polynomial in (7) is irreducible over the reals. Thus while its three roots are real, they require complex numbers to be expressed in radicals¹¹⁰.
- ⁴¹T. R. Auton, "The lift force on a spherical body in a rotational flow," *Journal of Fluid Mechanics* **183**, 199–218 (1987).
- ⁴²F. J. Beron-Vera, A. Hadjighasem, Q. Xia, M. J. Olascoaga, and G. Haller, "Coherent Lagrangian swirls among submesoscale motions," *Proc. Natl. Acad. Sci. U.S.A.* **Mar 2018**, 201701392 (2018).
- ⁴³L. Montabone, *Vortex Dynamics and Particle Transport in Barotropic Turbulence*, Ph.D. thesis, University of Genoa, Italy (2002).
- ⁴⁴K. L. Henderson, D. R. Gwynllwy, and C. F. Barenghi, "Particle tracking in Taylor–Couette flow," *European Journal of Mechanics - B/Fluids* **26**, 738 – 748 (2007).
- ⁴⁵T. P. Sapsis, N. T. Ouellette, J. P. Gollub, and G. Haller, "Neutrally buoyant particle dynamics in fluid flows: Comparison of experiments with lagrangian stochastic models," *Physics of Fluids* **23**, 093304 (2011).
- ⁴⁶M. Farazmand and G. Haller, "The Maxey–Riley equation: Existence, uniqueness and regularity of solutions," *Nonlinear Analysis: Real World Applications* **22**, 98–106 (2015).
- ⁴⁷G. P. Langlois, M. Farazmand, and G. Haller, "Asymptotic dynamics of inertial particles with memory," *Journal of Nonlinear Science* **25**, 1225–1255 (2015).
- ⁴⁸A. Daitche and T. Tél, "Memory effects are relevant for chaotic advection of inertial particles," *Phys. Rev. Lett.* **107**, 244501 (2011).
- ⁴⁹A. Daitche and T. Tél, "Memory effects in chaotic advection of inertial particles," *New Journal of Physics* **16**, 073008 (2014).
- ⁵⁰M. Sudharsan, S. L. Brunton, and J. J. Riley, "Lagrangian coherent structures and inertial particle dynamics," *Phys. Rev. E* **93**, 033108 (2016).
- ⁵¹In an earlier geophysical adaptation of the Maxey–Riley equation¹², the centrifugal force was included as well, but this is actually balanced out by the gravitational force on the horizontal plane.
- ⁵²J. Pedlosky, *Geophysical Fluid Dynamics*, 2nd ed. (Springer, 1987) p. 624 pp.
- ⁵³P. Ripa, "'Inertial' oscillations and the β -plane approximation(s)," *J. Phys. Oceanogr.* **27**, 633–647 (1997).
- ⁵⁴J. Röhrs, K. H. Christensen, L. R. Hole, G. Broström, M. Drivdal, and S. Sundby, "Observation-based evaluation of surface wave effects on currents and trajectory forecasts," *Ocean Dyn.* **62**, 1519–1533 (2012).
- ⁵⁵O. Nesterov, "Consideration of various aspects in a drift study of MH370 debris," *Ocean Sci.* **14**, 387–402 (2018).
- ⁵⁶A. Sozza, F. De Lillo, S. Musacchio, and G. Boffetta, "Large-scale confinement and small-scale clustering of floating particles in stratified turbulence," *Physical Review Fluids* **1**, 052401(R) (2016).
- ⁵⁷Ø. Breivik and A. Allen, "An operational search and rescue model for the Norwegian Sea and the North Sea," *J. Marine Syst.* **69**, 99–113 (2008).
- ⁵⁸A. V. Duhec, R. F. Jeanne, N. Maximenko, and J. Hafner, "Composition and potential origin of marine debris stranded in the Western Indian Ocean on remote Alphonse Island, Seychelles," *Mar. Poll. Bull.* **96**, 76–86 (2015).
- ⁵⁹M. R. Allshouse, G. N. Ivey, R. J. Lowe, N. L. Jones, C. Beeglekrause, J. Xu, and T. Peacock, "Impact of windage on ocean surface lagrangian coherent structures," *Environmental Fluid Mechanics* **17**, 473–483 (2017).
- ⁶⁰W. R. Geyer, "Field calibration of mixed-layer drifters," *Journal of Atmospheric and Oceanic Technology* **6**, 333–342 (1989), [https://doi.org/10.1175/1520-0426\(1989\)006j0333:FCOMLDj2.0.CO;2](https://doi.org/10.1175/1520-0426(1989)006j0333:FCOMLDj2.0.CO;2).
- ⁶¹P. K. Kundu, I. M. Cohen, and D. R. Dowling, *Fluid Mechanics*, 5th ed. (Academic Press, 2012) p. 891.
- ⁶²P. Daniel, G. Jan, F. Cabioch, Y. Landau, and E. Loiseau, "Drift modeling of cargo containers," *Spill Science & Technology Bulletin* **7**, 279 – 288 (2002).
- ⁶³T. Sapsis and G. Haller, "Instabilities in the dynamics of neutrally buoyant particles," *Physics of Fluids* **20**, 017102 (2008).

- ⁶⁴M.-H. Rio, S. Guinehut, and L. Gilles, “New CNES–CLS09 global mean dynamic topography computed from the combination of GRACE data, altimetry, and in situ measurements,” *Journal of Geophysical Research* **116**, C07018 (2011).
- ⁶⁵P.-Y. Le Traon, D. Antoine, A. Bentamy, H. Bonekamp, L. Breivik, B. Chapron, G. Corlett, G. Dibarboure, P. DiGiacomo, C. Donlon, Y. Faugere, J. Font, F. Girard-Ardhuin, F. Gohin, J. Johannessen, M. Kamachi, G. Lagerloef, J. Lambin, G. Larnicol, P. L. Borgne, E. Leuliette, E. Lindstrom, M. Martin, E. Maturi, L. Miller, L. Mingsen, R. Morrow, N. Reul, M. Rio, H. Roquet, R. Santoleri, and J. Wilkin, “Use of satellite observations for operational oceanography: recent achievements and future prospects,” *Journal of Operational Oceanography* **8**, s12–s27 (2015).
- ⁶⁶As is well-accepted, such an η is a reflection mainly of the first baroclinic mode in the ocean¹¹¹, wherein the sea surface is effectively a horizontally rigid surface with the main thermocline displacing vertically from equilibrium by $-g\eta/g'$, where $g' \approx 10^{-3}g$ is the buoyancy jump across it¹¹². Thus considering altimetry-derived currents is not at odds with our flat surface assumption.
- ⁶⁷G. Haller and T. Sapsis, “Where do inertial particles go in fluid flows?” *Physica D* **237**, 573–583 (2008).
- ⁶⁸The asymptotic dynamics of the original Maxey–Riley set, assuming a steady carrying flow, was first investigated by Rubin, Jones, and Maxey¹¹³, in the context of the settling of negatively buoyant (i.e., heavy or aerosol) particles in convection cells, problem originally investigated by Stommel¹¹⁴ ignoring inertial effects. Additional $\tau \rightarrow 0$ asymptotic dynamics investigations of the standard Maxey–Riley set followed^{115,116}, also in an autonomous setting.
- ⁶⁹M. J. Olascoaga, F. J. Beron-Vera, L. E. Brand, and H. Koçak, “Tracing the early development of harmful algal blooms on the West Florida Shelf with the aid of Lagrangian coherent structures,” *J. Geophys. Res.* **113**, C12014 (2008).
- ⁷⁰N. Fenichel, “Geometric singular perturbation theory for ordinary differential equations,” *J. Differential Equations* **31**, 51–98 (1979).
- ⁷¹The slow manifold \mathcal{S}_τ and the Maxey–Riley equation restricted to \mathcal{S}_τ formally satisfy the definition of *inertial manifold* and *inertial equation*, respectively, developed in the study of long-time-asymptotic behavior (attractors) of infinite-dimensional dynamical systems¹¹⁷. In such systems, actual attractors are hard to compute and are generally not even manifolds. The inertial manifold is easier to compute, smooth, and contains the attractor. It is unclear to us why these constructs are called “inertial,” but this certainly is not related to resistance of an object to a change in its velocity as meant here.
- ⁷²G. Peng, H.-M. Zhang, H. P. Frank, J.-R. Bidlot, M. Higgaki, S. Stevens, and W. R. Hankins, “Evaluation of various surface wind products with OceanSITES buoy measurements,” *Weather and Forecasting* **28**, 1281–1303 (2013), <https://doi.org/10.1175/WAF-D-12-00086.1>.
- ⁷³F. J. Beron-Vera, “Preferential sampling of elastic inertial chains in the ocean,” Preprint (2019).
- ⁷⁴R. Lumpkin and M. Pazos, “Measuring surface currents with Surface Velocity Program drifters: the instrument, its data and some recent results,” in *Lagrangian Analysis and Prediction of Coastal and Ocean Dynamics*, edited by A. Griffa, A. D. Kirwan, A. Mariano, T. Özgökmen, and T. Rossby (Cambridge University Press, 2007) Chap. 2, pp. 39–67.
- ⁷⁵P. P. Niiler and J. D. Paduan, “Wind-driven Motions in the northeastern Pacific as measured by Lagrangian drifters,” *J. Phys. Oceanogr.* **25**, 2819–2830 (1995).
- ⁷⁶L. Lebreton, B. Slat, F. Ferrari, B. Sainte-Rose, J. Aitken, R. Marthouse, S. Hajbane, S. Cunsolo, A. Schwarz, A. Levivier, K. Noble, P. Debeljak, H. Maral, R. Schoeneich-Argent, R. Brambini, and J. Reisser, “Evidence that the great pacific garbage patch is rapidly accumulating plastic,” *Scientific Reports* **8**, 4666 (2018).
- ⁷⁷H. Stommel, “The westward intensification of wind-driven ocean currents,” *Trans. AGU* **29**, 202–206 (1948).
- ⁷⁸D. B. Haidvogel and F. Bryan, “Climate system modeling,” (Oxford Press, 1992) Chap. Ocean general circulation modeling, pp. 371–412.
- ⁷⁹W. G. Large and S. Pond, “Open ocean momentum flux measurements in moderate to strong winds,” *Journal of Physical Oceanography* **11**, 324–336 (1981).
- ⁸⁰M. van der Mheen, C. Pattiaratchi, and E. van Sebille, “Role of indian ocean dynamics on accumulation of buoyant debris,” *Journal of Geophysical Research: Oceans* **124**, doi:10.1029/2018JC014806 (2019), <https://agupubs.pericles-prod.literatumonline.com/doi/pdf/10.1029/2018JC014806>.
- ⁸¹J. A. Cummings and O. M. Smedstad, “Variational data analysis for the global ocean,” in *Data Assimilation for Atmospheric, Oceanic and Hydrologic Applications*, Vol. 2, edited by S. K. Park and L. Xu (Springer-Verlag Berlin Heidelberg, 2013) Chap. 13.
- ⁸²S. A. Hsu, E. A. Meindl, and D. B. Gilhousen, “Determining the power-law wind-profile exponent under near-neutral stability conditions at sea,” *J. App. Met.* **33**, 757–756 (1994).
- ⁸³G. Froyland, R. M. Stuart, and E. van Sebille, “How well-connected is the surface of the global ocean?” *Chaos* **24**, 033126 (2014).
- ⁸⁴P. Miron, F. J. Beron-Vera, M. J. Olascoaga, J. Sheinbaum, P. Pérez-Brunius, and G. Froyland, “Lagrangian dynamical geography of the Gulf of Mexico,” *Scientific Reports* **7**, 7021 (2017).
- ⁸⁵P. Miron, F. J. Beron-Vera, M. J. Olascoaga, G. Froyland, P. Pérez-Brunius, and J. Sheinbaum, “Lagrangian geography of the deep Gulf of Mexico,” *J. Phys. Oceanogr.* **49**, 269–290 (2018).
- ⁸⁶M. J. Olascoaga, P. Miron, C. Paris, P. Pérez-Brunius, R. Pérez-Portela, R. H. Smith, and A. Vaz, “Connectivity of Pulley Ridge with remote locations as inferred from satellite-tracked drifter trajectories,” *Journal of Geophysical Research* **123**, 5742–5750 (2018).
- ⁸⁷J. H. LaCasce, “Statistics from Lagrangian observations,” *Progr. Oceanogr.* **77**, 1–29 (2008).
- ⁸⁸A. N. Maximenko, J. Hafner, and P. Niiler, “Pathways of marine debris derived from trajectories of Lagrangian drifters,” *Mar. Pollut. Bull.* **65**, 51–62 (2012).
- ⁸⁹E. van Sebille, E. H. England, and G. Froyland, “Origin, dynamics and evolution of ocean garbage patches from observed surface drifters,” *Environ. Res. Lett.* **7**, 044040 (2012).
- ⁹⁰G. H. Ganser, “A rational approach to drag prediction of spherical and nonspherical particles,” *Powder Technology* **77**, 143–152 (1993).
- ⁹¹J. C. McWilliams, “Fluid dynamics at the margin of rotational control,” *Environ. Fluid Mech.* **8**, 441–449 (2008).
- ⁹²R. B. Fitzgerald, D. J. Finlayson, and A. Allen, “Drift of common search and rescue objects - Phase III.” Report, Canadian Coast Guard, Canadian Coast Guard, Research and Development, Ottawa. (1994).
- ⁹³O. M. Phillips, *Dynamics of the Upper Ocean* (Cambridge University Press, 1997).
- ⁹⁴G. Broström, K. H. Christensen, and J. E. H. Weber, “A quasi-Eulerian, quasi-Lagrangian view of surface-wave-induced flow in the ocean,” *J. Phys. Oceanogr.* **38**, 1122–1130 (2008), <https://doi.org/10.1175/2007JPO3702.1>.
- ⁹⁵K. Hasselmann, “Wave-driven inertial oscillations,” *Geophys. Fluid Dyn.* **1**, 463–502 (1970).
- ⁹⁶Ø. Breivik, K. Mogenssen, J.-R. Bidlot, M. A. Balmaseda, and P. A. E. M. Janssen, “Surface wave effects in the nemo ocean model: Forced and coupled experiments,” *J. Geophys. Res.* **120**, 2973–2992 (2015).
- ⁹⁷A. D. D. Craik, “The drift velocity of water waves,” *J. Fluid Mech.* **116**, 187–205 (1982).
- ⁹⁸A. D. Jenkins, “The use of a wave prediction model for driving a near-surface current model,” *Ocean Dyn.* **42**, 133–149 (1989).

- ⁹⁹J. Wu, "Sea-surface drift currents induced by wind and waves," *J. Phys. Oceanogr.* **13**, 1441–1451 (1983), [https://doi.org/10.1175/1520-0485\(1983\)013;1441:SSDCIB;2.0.CO;2](https://doi.org/10.1175/1520-0485(1983)013;1441:SSDCIB;2.0.CO;2).
- ¹⁰⁰H. Tamura, Y. Miyazawa, and L.-Y. Oey, "The Stokes drift and wave induced-mass flux in the North Pacific," *J. Geophys. Res.* **117**, C08021 (2012).
- ¹⁰¹A. Webb and B. Fox-Kemper, "Wave spectral moments and Stokes drift estimation," *Ocean Modell.* **40**, 273–288 (2011).
- ¹⁰²A. Webb and B. Fox-Kemper, "Impacts of wave spreading and multidirectional waves on estimating Stokes drift," *Ocean Modelling* **96**, 49–64 (2015).
- ¹⁰³Ø. Breivik, J.-R. Bidlot, and P. A. Janssen, "A Stokes drift approximation based on the Phillips spectrum," *Ocean Modelling* **100**, 49 – 56 (2016).
- ¹⁰⁴A. Daitche, "Advection of inertial particles in the presence of the history force: Higher order numerical schemes," *J. Comput. Phys.* **254**, 93–106 (2013).
- ¹⁰⁵P. Tanga and A. Provenzale, "Dynamics of advected tracers with varying buoyancy," *Physica D* **76**, 202–215 (1994).
- ¹⁰⁶G. L. Pickard and W. J. Emery, *Descriptive Physical Oceanography. An Introduction* (Pergamon, 1990).
- ¹⁰⁷F. J. Beron-Vera, "Constrained-Hamiltonian shallow-water dynamics on the sphere," in *Nonlinear Processes in Geophysical Fluid Dynamics: A Tribute to the Scientific Work of Pedro Ripa*, edited by O. U. Velasco-Fuentes, J. Sheinbaum, and J. Ochoa (Kluwer, 2003) pp. 29–51.
- ¹⁰⁸P. Ripa, "Caída libre y la figura de la Tierra," *Rev. Mex. Fís.* **41**, 106–127 (1995).
- ¹⁰⁹P. Ripa, *La increíble historia de la malentendida fuerza de Coriolis (The Incredible Story of the Misunderstood Coriolis Force)* (Fondo de Cultura Económica, 1997).
- ¹¹⁰L. Wantzel, "Classification des nombres incommensurables d'origine algébrique," *Nouvelles Annales de Mathématiques: Journal des Candidats aux Écoles Polytechnique et Normale* **2**, 117–127 (1843).
- ¹¹¹C. Wunsch, "The vertical partition of oceanic horizontal kinetic energy," *J. Phys. Oceanogr.* **27**, 1770–1794 (1997).
- ¹¹²A. E. Gill, *Atmosphere-Ocean Dynamics* (Academic, 1982).
- ¹¹³J. Rubin, C. K. R. T. Jones, and M. Maxey, "Settling and asymptotic motion of aerosol particles in a cellular flow field," *J. Nonlin. Sci.* **5**, 337–358 (1995), [10.1007/BF01275644](https://doi.org/10.1007/BF01275644).
- ¹¹⁴H. J. Stommel, "Trajectories of small bodies sinking slowly through convection cells," *J. Mar. Res.* **8**, 24–29 (1949).
- ¹¹⁵T. J. Burns, R. W. Davis, and E. F. Moore, "A perturbation study of particle dynamics in a plane wake flow," *J. Fluid Mech.* **384**, 1–26 (1999).
- ¹¹⁶E. Mograbi and E. Bar-Ziv, "On the asymptotic solution of the MaxeyRiley equation," *Phys. Fluids* **18**, 051704 (2006).
- ¹¹⁷R. Temam, "Inertial manifolds," *The Mathematical Intelligencer* **12**, 68–74 (1990).